12-9-2022

NEDDylated Cullin 3 mediates the adaptive response to topoisomerase 1 inhibitors

Alice Meroni

Jan Grosser

Sumedha Agashe

Natasha Ramakrishnan

Jessica Jackson

See next page for additional authors

Authors

Alice Meroni, Jan Grosser, Sumedha Agashe, Natasha Ramakrishnan, Jessica Jackson, Priyanka Verma, Laura Baranello, and Alessandro Vindigni

Molecular biology

NEDDylated Cullin 3 mediates the adaptive response to topoisomerase 1 inhibitors

Alice Meroni[1], Jan Grosser[2], Sumedha Agashe[1], Natasha Ramakrishnan[1], Jessica Jackson[1], Priyanka Verma[1], Laura Baranello[2], Alessandro Vindigni[1]*

DNA topoisomerase 1 (TOP11) inhibitors are mainstays of anticancer therapy. These drugs trap TOP1 on DNA, stabilizing the TOP1-cleavage complex (TOP1-cc). The accumulation of TOP1-ccs perturbs DNA replication fork progression, leading to DNA breaks and cell death. By analyzing the genomic occupancy and activity of TOP1, we show that cells adapt to treatment with multiple doses of TOP1 inhibitor by promoting the degradation of TOP1-ccs, allowing cells to better tolerate subsequent doses of TOP1 inhibitor. The E3-RING Cullin 3 ligase in complex with the BTBD1 and BTBD2 adaptor proteins promotes TOP1-cc ubiquitination and subsequent proteasomal degradation. NEDDylation of Cullin 3 activates this pathway, and inhibition of protein NEDDylation or depletion of Cullin 3 sensitizes cancer cells to TOP1 inhibitors. Collectively, our data uncover a previously unidentified NEDD8–Cullin 3 pathway involved in the adaptive response to TOP1 inhibitors, which can be targeted to improve the efficacy of TOP1 drugs in cancer therapy.

INTRODUCTION

DNA topoisomerases play essential roles in maintaining the homeostasis of DNA topology, resolving topological stress generated by DNA replication, transcription, and chromatin remodeling (*1*). Topoisomerase 1 (TOP1) relaxes superhelical tension on the DNA by introducing a break in one of the two DNA strands and allowing one end to rotate freely to release torsional stress. At the same time, TOP1 stays covalently bound to the other DNA end and catalyzes the religation reaction as soon as the torsional stress is resolved. This intermediate state, commonly referred as the TOP1-cleavage complex (TOP1-cc), is extremely transient and thus not detectable in living cells (*2*, *3*).

TOP1 is specifically inhibited by camptothecin (CPT) (*4*, *5*), the prototype of several compounds widely used for cancer treatment (*6*). Topotecan and irinotecan are two CPT analogs approved by the U.S. Food and Drug Administration (FDA) for the treatment of colorectal, ovarian, and lung cancer (*7*). More recently, the FDA approved the use of a HER2-directed antibody conjugated to a different CPT analog (Enhertu) that specifically targets HER2-positive breast cancers and gastric adenocarcinomas (*8*–*10*). The efficacy of these inhibitors is often limited by the development of chemoresistance (*11*). As drug resistance is a major limitation of chemotherapy, defining the underlying mechanisms that govern drug response is key to develop novel and more effective anticancer strategies.

CPT selectively targets TOP1 when it is covalently bound to DNA as a TOP1-cc intermediate. The trapping of TOP1-cc by CPT results in the accumulation of detrimental DNA-protein adducts and single-strand DNA (ssDNA) breaks (*7*). These bulky protein-DNA adducts constitute an obstacle for DNA replication progression, leading to fork slowing and reversal (*12*, *13*). Moreover, the associated single-strand breaks can be converted into lethal double-strand breaks (DSBs) upon collision with the replication machinery (*14*, *15*). Because of this mechanism of action, CPT is particularly toxic to actively replicating cells (*16*–*18*).

Stabilized TOP1-ccs are repaired through different pathways (*19*). Tyrosyl-DNA phosphodiesterase 1 (TDP1) is a critical player in this process that cleaves the covalent bond between TOP1 and the DNA in TOP1-cc (*20*–*23*). Moreover, before being targeted by TDP1, TOP1-ccs need to be partially degraded by the proteasome (*24*), implying that TOP1-ccs are subject to ubiquitin conjugation as a degradation signal. Previous studies implicated the breast cancer type 1 susceptibility protein (BRCA1) and the E3 Cullin complexes in TOP1 ubiquitination (*25*–*27*). However, little is known about the mechanisms that control TOP1 ubiquitination. Once TOP1-cc has been cleared from the DNA, many factors contribute to the repair of the single-strand break, including XRCC1, PARP1, MRE11, CtIP, XPF, and XPG (*28*, *29*). Recently, nonproteasomal proteases have also been implicated in the repair of TOP1-ccs, although their exact function needs further investigation (*30*, *31*).

Most of the previous studies focused on how cells respond to treatment with a single dose of TOP1 inhibitor, neglecting the fact that cells can adapt to genotoxic stress and that patients are treated with multiple drug doses in clinical settings. For example, earlier studies showed that cells exposed to low doses of ultraviolet (UV) or ionizing radiation are able to better cope with a subsequent treatment with a higher radiation dose (*32*–*37*). Moreover, we recently demonstrated that BRCA-deficient cancer cells adapt to treatment with multiple cisplatin doses by up-regulating a specialized replication fork recovery pathway, called repriming (*38*). These studies highlighted how studying the effect of multiple drug doses is crucial to understanding how cells adapt to treatment with a specific drug and modulate cancer therapy response. However, the mechanism of adaptation to TOP1 inhibition has not been investigated yet.

In this work, we implemented a multiple dose scheme to study the adaptive response to TOP1 inhibitors. We treated cells with a low dose of TOP1 inhibitor—CPT—(called predose), followed by a second treatment with a higher dose (called challenging dose) 24 hours later. Using this experimental setup, we investigated the

[1]Division of Oncology, Department of Medicine, Washington University in St. Louis, St. Louis, MO 63110, USA. [2]Karolinska Institutet, CMB, 171 65 Solna, Sweden.
*Corresponding author. Email: avindigni@wustl.edu

adaptive response mechanism that allows cells to better cope with subsequent doses of TOP1 inhibitors. Genome-wide mapping of TOP1 upon treatment with the two CPT doses revealed decreased TOP1 binding at transcription start sites (TSSs) and early replication sites, as compared to cells treated with the challenging dose alone. Accordingly, we found that treatment with multiple CPT doses reduces the levels of TOP1-ccs and causes a concomitant reduction in the levels of DNA breaks and replication fork perturbations commonly detected upon treatment with a single dose of TOP1 inhibitors. Adaptation to CPT or other TOP1 inhibitors does not rely on TDP1, but it involves the degradation of TOP1-ccs mediated by the Cullin 3 (CUL3) E3 ubiquitin ligase in complex with the specific BTB domain containing 1 and 2 (BTBD1 and BTBD2) adaptor proteins. Moreover, we found that NEDDylation is crucial to activate CUL3 function and promote TOP1-cc degradation. In agreement with this model, we also found that suppression of this adaptive response mechanism by inhibition of protein NEDDylation or depletion of CUL3 sensitizes cancer cells to TOP1 inhibitors. These findings inspire an approach for chemotherapy regimens that combine TOP1 inhibitors with NEDDylation inhibitors.

RESULTS

Treatment with multiple CPT doses decreases TOP1 accumulation on DNA

To study the adaptive response to CPT, we implemented a multiple-dose scheme where we first treated human retinal pigment epithelial (RPE-1) cells with 25 nM CPT for 1 hour ("predose"; Fig. 1A), a condition that did not cause any significant cell cycle perturbation or reduced viability within 24 hours (fig. S1, A to C). Next, we allowed cells to adapt for 24 hours in the absence of the drug before challenging them with a higher concentration of CPT for 1 hour ("challenging dose," 0.1 or 1 μM; see Fig. 1A). Last, we collected all the samples at the same time after the challenging dose for the follow-up experiments.

Being TOP1 the unique target of CPT (*4*), we first looked at its genomic distribution and occupancy by chromatin immunoprecipitation sequencing (ChIP-seq) in RPE-1 cells, comparing the relative response to the CPT challenging dose in the presence or absence of the predose. The ChIP-seq approach detects TOP1 bound on chromatin, regardless of whether it is covalently engaged with the DNA (TOP1-cc) or not (fig. S1D). TOP1 binding is prominent at TSSs, and addition of CPT traps and stabilizes TOP1-ccs, resulting in an increased TOP1 ChIP-seq signal (*39*). Accordingly, we found that treatment with the challenging dose alone led to an increase in TOP1 occupancy at TSSs relative to the untreated sample (Fig. 1B and fig. S1, E and F, for tracks at selected genes) while not changing the overall distribution of the enzyme along the gene bodies (fig. S1G). Contrarily to what was detected by treating cells solely with the challenging dose, treatment with predose + challenging dose caused a decrease in TOP1 binding at TSSs relative to the cells treated with the predose alone (Fig. 1C, fig. S1, E and F, for tracks at selected genes, and fig. S1G). These data suggest that the cellular response to the challenging dose of CPT is different when cells are "primed" with the predose.

As DNA topology plays an important role in the replication process and low doses of CPT perturb DNA replication (*13*, *40*), we analyzed TOP1 binding in relation to replication timing. We used publicly available Repli-seq datasets from RPE-1 cells to identify early and late replicated domains (*41*). The analysis of TOP1 binding at early versus late replicated regions revealed a clear skew of TOP1 occupancy on the early replicated sequences (Fig. 1, D and E, and fig. S1, H and I, for tracks at selected domains). This is in line with the notion that early DNA replication occurs within actively transcribed chromatin (*42*, *43*), which is preferentially bound by TOP1 (*39*). TOP1 could assist replication origin firing (*44*) and/or fork progression by removing supercoiling ahead of the DNA polymerase (*45*). Because of the size of the regions analyzed (1 MB on average), the resolution of Repli-seq does not allow to appreciate clear differences between CPT treatments. Thus, we used publicly available Okazaki fragment sequencing (OK-seq) datasets in RPE-1 cells (*41*, *46*) to identify replication initiation sites within the early replicating domains previously identified by Repli-seq. The curated list contained about 2900 replication initiation sites, which were used for the downstream analysis. Inspecting TOP1 binding at these regions revealed a sharp peak centered around the initiation sites (Fig. 1F), although we cannot exclude that TOP1 enrichment at these sites is due to TOP1 association with TSSs. Treatment with the CPT challenging dose alone increased TOP1 enrichment at the initiation sites compared to the untreated sample (Fig. 1F). In contrast, treatment with the predose + challenging dose caused a decrease in the TOP1 signal compared to the predose alone (Fig. 1G), similarly to the results obtained at TSSs (Fig. 1, B and C). To highlight the effect of the predose on the cellular response to the challenging dose, we compared the ratios between the TOP1 ChIP-seq profiles after challenging dose and untreated (red curve in Fig. 1H) versus predose + challenging dose and predose alone (orange curve in Fig. 1H). A marked reduction in the fraction of TOP1 stabilized by the challenging dose was observed when cells were primed with the predose (Fig. 1H). Altogether, these data suggest that cells adapt to treatment with the CPT predose by modulating the amount of TOP1 bound to chromatin, at both TSSs and early replication initiation sites.

The adaptive response to CPT lowers the levels of TOP1-ccs

Because ChIP-seq only assesses the total amount of TOP1 bound to DNA—either engaged or not in a cleavage complex with DNA—we used the Rapid Approach for DNA Adduct Recovery (RADAR) assay to specifically measure the amount of TOP1-ccs (fig. S1D) (*47*, *48*). TOP1-cc is a short-lived intermediate, and it is barely detectable if not stabilized by CPT. This can be observed both in the untreated conditions and in the cells treated only with predose, leading to comparably low TOP1-cc levels (Fig. 2A). Notably, while the RADAR assay did not detect a significant increase in TOP1-ccs 24 hours after predose compared to untreated cells (Fig. 2, A and B, and fig. S2A for RADAR DNA loading control), the ChIP-seq assay revealed increased TOP1 occupancy 24 hours after predose treatment, compared to the untreated sample (Fig. 1, B and C, and fig. S1G, compare orange versus red curve). These data suggest that the predose alone does not lead to an increase in the TOP1-cc levels but only to an increase of TOP1 bound to DNA (Fig. 1B), allowing a direct comparison between the TOP1-cc levels of samples treated with the challenging dose alone and samples treated with predose + challenging dose. We found that while the challenging dose alone increased TOP1-ccs, consistent with the ChIP-seq results (Fig. 1B), the combination of the predose + challenging dose lowered TOP1-ccs compared to the

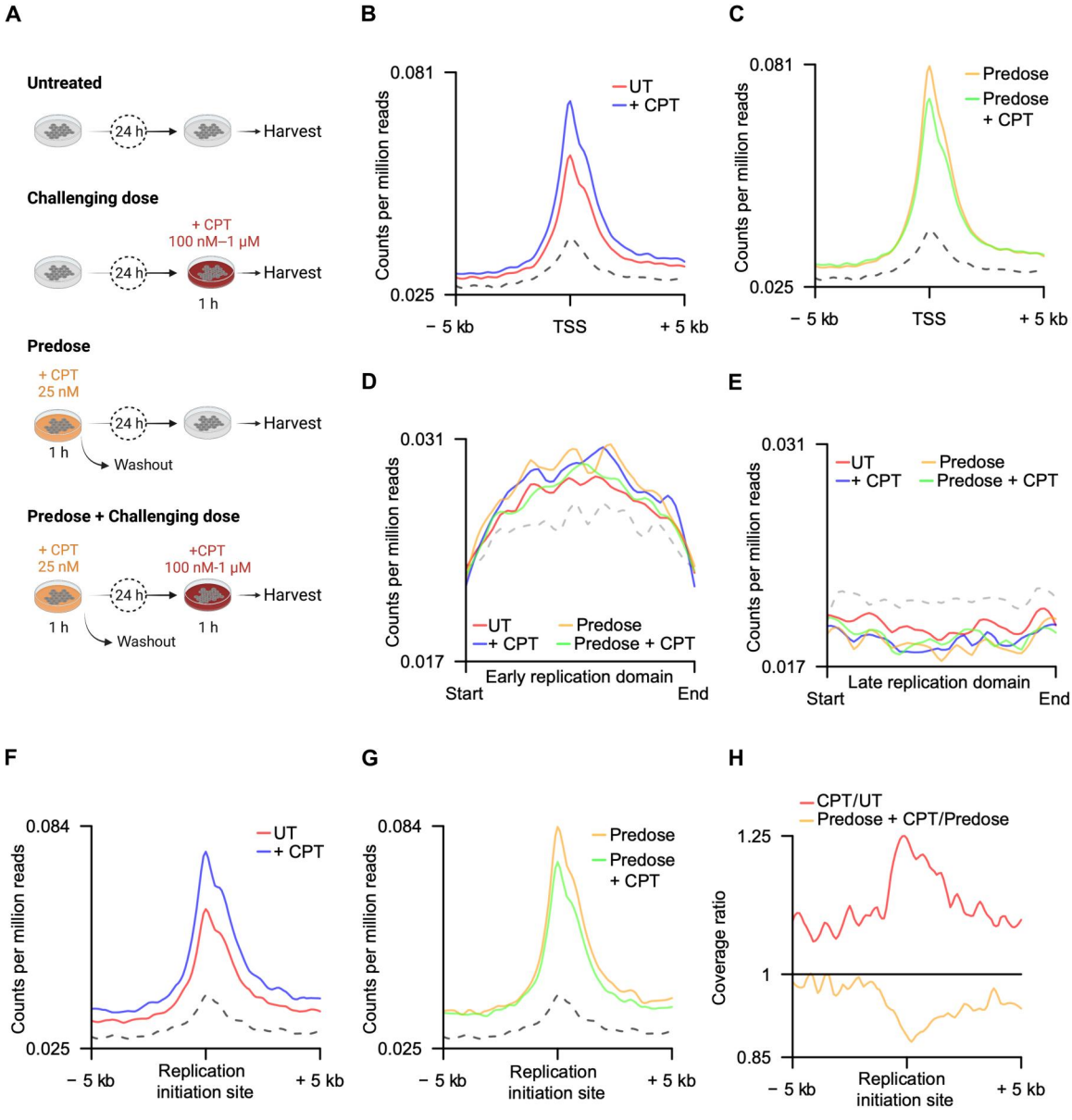

Fig. 1. Adaptive response to CPT decreases TOP1 bound to DNA without affecting TOP1 distribution genome wide. (**A**) CPT treatment scheme. (**B**) TOP1 occupancy (expressed as counts per million reads) at TSSs ± challenging dose (1 μM CPT, 1 hour). − 5 kb and + 5 kb indicate reads within 5 kb upstream or downstream of TSS. Dashed line indicates the input sample. Significance between challenging dose treated versus untreated samples for TOP1 was calculated using a Wilcoxon rank-sum test. $P \leq 0.0001$ comparing means of average signal ± 500-bp window around TSS. (**C**) TOP1 occupancy (expressed as counts per million reads) at TSS in cells treated with the predose (25 nM CPT, 1 hour) ± challenging dose (1 μM CPT, 1 hour). − 5 kb and + 5 kb indicate reads within 5 kb upstream or downstream of TSS. Dashed line indicates the input sample. Significance between predose + challenging dose treated versus predose treated samples for TOP1 was calculated as in (B). $P \leq 0.0001$. (**D**) TOP1 enrichment at early and (**E**) at late replication domains detected by Repli-seq ± predose and ± challenging dose. (**F**) TOP1 enrichment at replication initiation sites ± challenging dose (1 μM CPT, 1 hour). Dashed line indicates the input sample. Significance between challenging dose treated versus untreated samples for TOP1 was calculated as in (B). $P \leq 0.0001$. (**G**) TOP1 enrichment at replication initiation sites in cells treated with the predose (25 nM CPT, 1 hour) ± challenging dose (1 μM CPT, 1 hour). Significance between predose + challenging dose treated versus predose treated samples for TOP1 was calculated as in (B). $P \leq 0.0001$. (**H**) Relative enrichment of TOP1 at replication origins. The plot shows the ratio of ChIP-seq reads detected in the CPT-treated sample (challenging dose) to its relative control.

challenging dose alone (Fig. 2, A and B, and fig. S2A for RADAR DNA loading control). The total expression level of TOP1 did not vary upon the different CPT treatments (Fig. 2C), suggesting that the adaptive response to CPT only affects the levels of TOP1 bound to DNA or engaged in a TOP1-cc.

Because TDP1 is key for the repair of TOP1-ccs, responsible for cleaving the covalent bond between TOP1 and the DNA (*20*–*23*), we tested whether the adaptive response to CPT was TDP1 dependent. We measured TOP1-cc accumulation and total TOP1 levels in RPE-1 TDP1 knockout (TDP1 KO) cells. Similar to the results obtained in RPE-1 wild-type (WT) cells, we found that treatment of TDP1

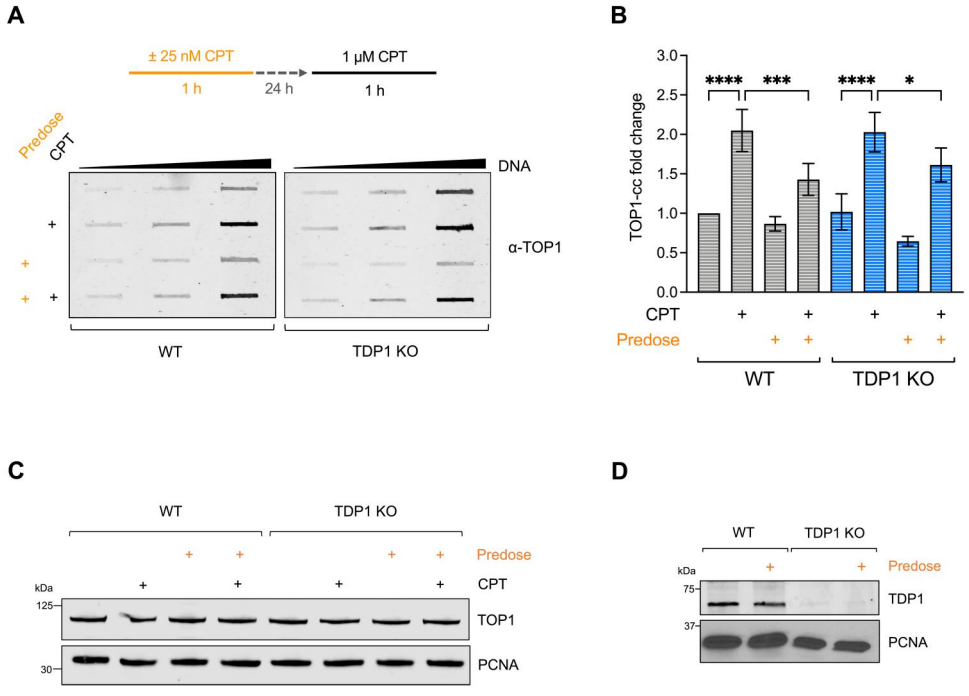

Fig. 2. The adaptive response to CPT lowers the levels of TOP1-ccs, independently of TDP1. (**A**) Top: Experimental scheme for the RADAR assay ± predose (25 nM CPT) and ± challenging dose (1 μM CPT). Bottom: Representative RADAR assay to measure TOP1-covalent complexes in WT and TDP1 KO cells. (**B**) RADAR assay quantification of TOP1-ccs; values are normalized relative to the untreated WT control and plotted as TOP1-cc fold change mean ± SEM ($N = 3$). Repeated-measures (RM) one-way analysis of variance (ANOVA), $^{*}P \leq 0.05$, $^{***}P \leq 0.001$, and $^{****}P \leq 0.0001$. (**C**) Total cellular TOP1 levels in WT and TDP1 KO cells ± predose (25 nM CPT) and ± challenging dose (1 μM CPT). (**D**) Total cellular Tdp1 levels in WT and TDP1 KO cells 24 hours after treatment with the ± predose (25 nM CPT).

KO cells with the predose + challenging dose led to a decrease in the levels of TOP1-cc compared to the challenging dose alone without affecting the total levels of TOP1 (Fig. 2, A to C, and fig. S2A for RADAR DNA loading control). In addition, we assessed TDP1 protein levels by Western blot and found that the total levels of TDP1 did not change 24 hours after treatment with the predose alone (Fig. 2D). Collectively, these data suggest that the adaptive response to CPT is not linked to changes in TDP1 expression, and it does not depend on the TDP1-mediated repair of TOP1-ccs.

To test whether the adaptive response to CPT triggers more general changes in gene expression, we performed differential expression analysis comparing RNA sequencing (RNA-seq) data from untreated versus cells treated only with predose and harvested 24 hours later (Fig. 1A). However, we did not detect any significant change in gene expression between the two conditions (fig. S2B), suggesting that the cellular adaptation to CPT treatment is not triggered by changes in the cellular transcriptome.

The adaptive response to CPT reduces replication stress and DNA damage

Previous studies indicate that TOP1 inhibition by CPT delays replication fork progression (*13*). We posited that if cells adapt to multiple CPT doses by reducing the net amount of TOP1-ccs during the challenging dose, this should attenuate the replication delays previously observed upon a single CPT treatment. To test this hypothesis, we used the DNA fiber assay, in which we first pulse-labeled RPE-1 cells with the thymidine analog 5-iodo-2′-deoxyuridine (IdU; red), for 20 min, followed by labeling with the second thymidine analog 5-chloro-2′-deoxyuridine (CldU; green), for 1 hour, in the presence of 100 nM CPT (Fig. 3A). In agreement with a previous study (*13*), we observed that treatment with the challenging CPT dose alone induced DNA replication fork slowing (Fig. 3A, compare lanes 1 and 3). Next, we pretreated cells with the CPT predose (25 nM) 24 hours before thymidine labeling and treatment with the challenging dose (Fig. 3A). While treatment with 25 nM CPT was previously shown to induce fork slowing immediately after drug treatment (*13*), we observed that pretreatment with 25 nM CPT 24 hours before fiber labeling did not affect fork progression (Fig. 3A, compare lanes 1 and 2). However, treatment with the predose + challenging dose reduced the replication fork slowing phenotype observed upon treatment with challenging dose alone (Fig. 3A, compare lanes 3 and 4). In the absence of TDP1, the replication fork slowing induced by the challenging dose alone was even more pronounced compared to WT cells (Fig. 3A, compare lanes 3 and 7). However, the replication slowing phenotype was rescued in the presence of the predose + challenging dose (Fig. 3A, compare lanes 7 and 8), mirroring the results obtained in TDP1-proficient cells. To statistically compare the differences between the samples treated with the challenging dose alone versus the samples treated with the predose + challenging dose, we also represented the results of the DNA fiber assay as a percentage of DNA replication fork progression in CPT treated relative to untreated cells (Fig. 3B). We found that this value was reduced to approximately 70% when WT cells were treated with the challenging dose alone. However, the fork progression rates were only reduced to approximately 87% upon addition of the predose (Fig. 3B). In TDP1 KO cells, the fork progression rates were reduced to 57% by treatment with the challenging dose alone and

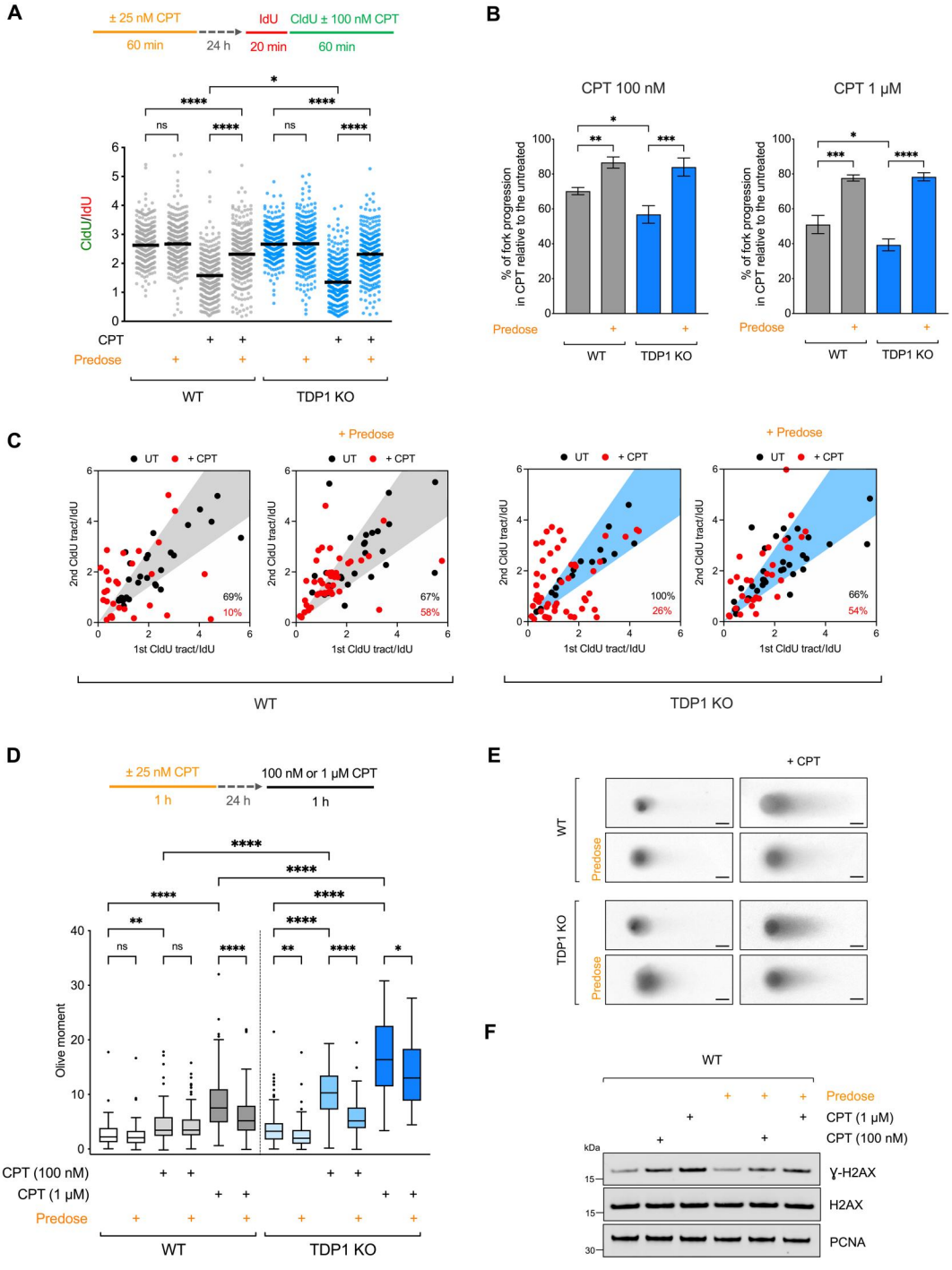

Fig. 3. The adaptive response to CPT reduces replication stress and DNA damage. (**A**) Top: Experimental scheme for the DNA fiber assay ± predose (25 nM CPT) and ± challenging dose (100 nM CPT). Bottom: Dot plot and median of CldU/IdU ratios in WT and TDP1 KO cells ($N = 3$). Kruskal-Wallis test; ns, nonsignificant, $^{*}P \leq 0.05$ and $^{****}P \leq 0.0001$. (**B**) Mean ± SEM of % of DNA replication progression in CPT treated relative to untreated WT and TDP1 KO cells ($N = 3$). Treatment was performed following the scheme of (A) and using 100 nM or 1 μM CPT as challenging dose. The % values were calculated by dividing the CldU/IdU median values of the CPT-treated samples by the corresponding values of the untreated samples. RM one-way ANOVA, $^{*}P \leq 0.05$, $^{**}P \leq 0.01$, $^{***}P \leq 0.001$, and $^{****}P \leq 0.0001$. (**C**) Scatterplot of newly fired origins in WT and TDP1 KO cells ± predose (25 nM CPT) and ± challenging dose (100 nM CPT). Each dot represents a single origin; the *X* and *Y* coordinates correspond to the CldU/IdU ratio of either fork origin arms (arbitrarily designated as first and second tracts). The shaded area represents a ratio of ≥0.7 between the two tracts, indicative of symmetric forks. Percentages in the right corner indicate total symmetric forks. (**D**) Top: Experimental scheme for the neutral comet assay ± predose (25 nM CPT) ± challenging dose (100 nM or 1 μM CPT). Bottom: Representative pictures of single comets from the neutral comet assay in WT and TDP1 KO cells. (**E**) DSBs quantification represented with a box-and-whisker Tukey plot of the olive moment from the neutral comet assay ($N = 3$, ≥150 cells analyzed for each experiment). Kruskal-Wallis test, $^{*}P \leq 0.05$, $^{**}P \leq 0.01$, and $^{****}P \leq 0.0001$. Scale bars, 20 μm. (**F**) Western blot of γ-H2AX and total H2AX in WT cells treated ± predose (25 nM CPT) ± challenging dose (100 nM or 1 μM CPT) ($N = 2$).

rescued to approximately 84% in the presence of the predose + challenging dose (Fig. 3B). Notably, we obtained similar results when we treated both cell lines with a higher concentration of CPT (1 μM) as challenging dose (Fig. 3B). The same results were also confirmed in colon cancer (RKO) and human osteosarcoma (U2OS) cells, indicating that the observed adaptive response phenotype is not cell type specific (fig. S3, A and B).

Treatment with DNA-damaging agents such as TOP1 inhibitors induces asymmetry at preexisting replication forks (*49*). This happens because the probability of simultaneously trapping TOP1-ccs on both sides of the fired origins is lower compared to trapping TOP1-ccs only on one side at any given time. In agreement with these findings, treatment with the challenging CPT dose alone led to a decrease in the percentage of symmetric forks from 69 to 10% when comparing untreated versus CPT-treated cells (Fig. 3C). However, replication fork symmetry increased to 58% in the presence of the predose + challenging dose (Fig. 3C). Similar results were obtained with the TDP1 KO cells (Fig. 3C).

Collectively, these results suggest that the reduction in TOP1-ccs induced by the addition of the CPT predose decreases the perturbations in replication fork dynamics caused by treatment with the challenging dose alone and rescues replication fork progression. This adaptive phenotype is specific for TOP1 inhibitors, as it was

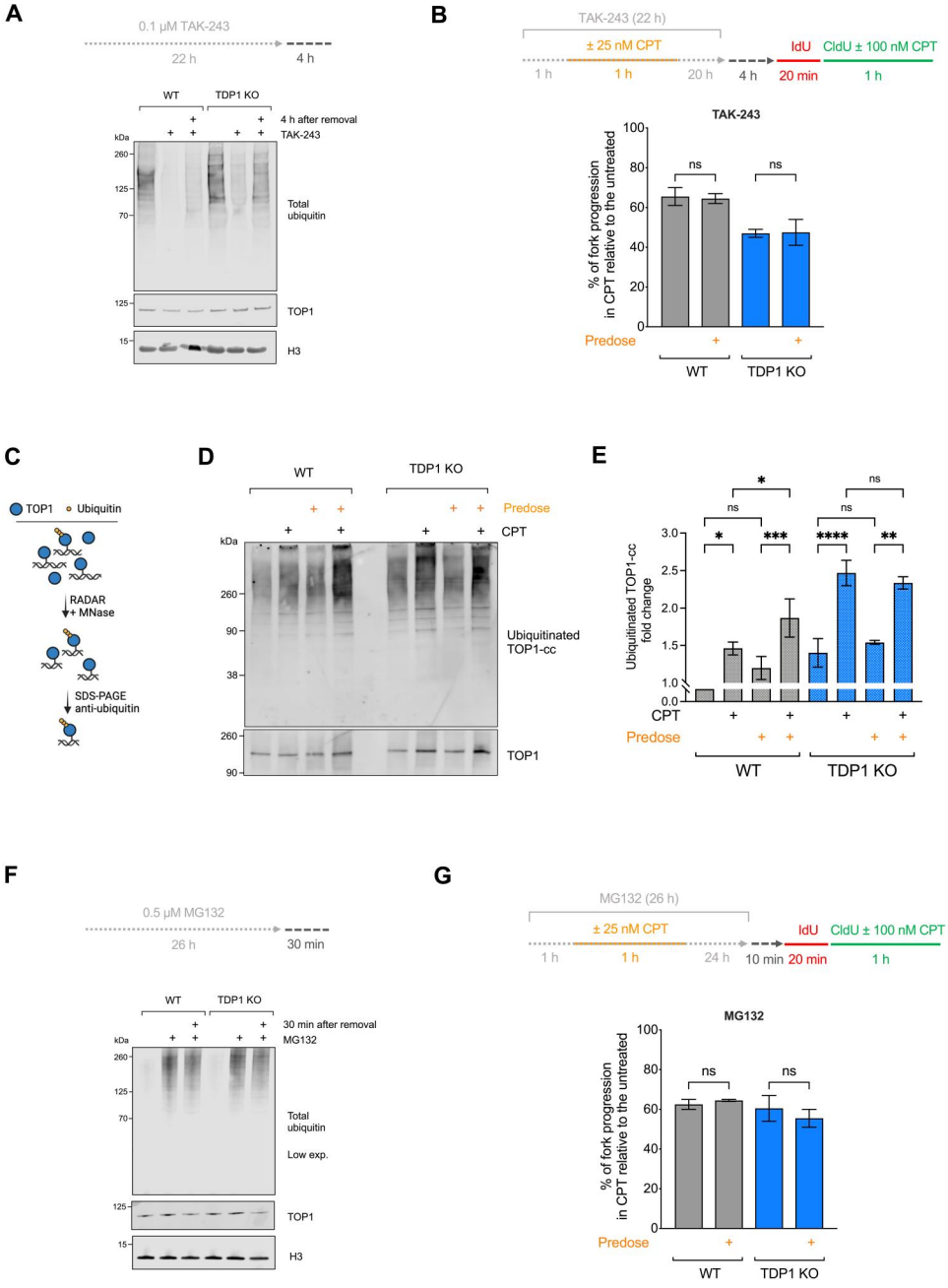

Fig. 4. The decrease in TOP1-cc is dependent on protein ubiquitination. (**A**) Top: TAK-243 inhibition scheme. Bottom: Western blot of total ubiquitin and total TOP1 in WT and TDP1 KO cells treated with 0.1 μM TAK-243 for 22 and 4 hours after its removal. (**B**) Top: Scheme for the DNA fiber assay with the TAK-243 inhibitor ± predose (25 nM CPT) and ± challenging dose (100 nM CPT). TAK-243 (0.1 μM) was added 1 hour before the predose and removed 4 hours before the DNA fiber assay. Bottom: Mean ± SEM of % of DNA replication progression in CPT treated relative to untreated WT and TDP1 KO cells ($N = 3$). RM one-way ANOVA. (**C**) Scheme for TOP1-cc ubiquitination assay. MNase, micrococcal nuclease. (**D**) Representative Western blot of TOP1-cc ubiquitination assay in WT and TDP1 KO ± predose (25 nM CPT) and ± challenging dose (1 μM CPT). (**E**) Mean ± SEM of the quantified ubiquitinated TOP1-cc signal relative to WT untreated control in WT and TDP1 KO cells ($N = 3$). RM one-way ANOVA, $^{*}P \leq 0.05$, $^{**}P \leq 0.01$, $^{***}P \leq 0.001$, and $^{****}P \leq 0.0001$. (**F**) Top: MG132 inhibition scheme. Bottom: Western blot of total ubiquitin and total TOP1 in WT and TDP1 KO cells treated with 0.5 μM MG132 for 26 hours and 30 min after its removal. (**G**) Top: Scheme for the DNA fiber assay with the MG132 inhibitor ± predose (25 nM CPT) and ± challenging dose (100 nM CPT). MG132 (0.5 μM) was added 1 hour before the predose and removed 10 min before the DNA fiber assay. Bottom: Mean ± SEM of % of DNA replication progression in CPT treated relative to untreated WT and TDP1 KO cells ($N = 2$). RM one-way ANOVA.

not detected using UV-C radiation as predose or as challenging dose (fig. S3, C and D).

Recent studies, including our own work, suggested that cells can rescue DNA replication fork slowing by repriming, which allows resumption of DNA synthesis downstream of DNA lesions (*38*, *50*, *51*). To test whether this mechanism is also involved in the rescue in fork progression observed upon treatment with multiple CPT doses, we used the ssDNA-specific S1 nuclease to determine whether the CldU-labeled tracts contained ssDNA gaps that would form upon repriming (*52*). However, we could not detect any change in gap formation associated with multiple CPT doses (fig. S3E). Similar results were obtained using a nondenaturing immunofluorescence approach that directly monitors ssDNA gap accumulation (fig. S3F) (*53*), suggesting that cells do not use repriming to rescue replication fork progression under these conditions. Moreover, we found that depletion of RAD18, an E3 ubiquitin ligase that plays a central role in translesion synthesis (TLS) by promoting proliferating cell nuclear antigen (PCNA) mono-ubiquitination and the downstream recruitment of TLS polymerases (*54*), did not rescue fork progression under the same conditions, suggesting that TLS is also not involved in the adaptive response to CPT (fig. S3, F and G).

CPT generates single-strand breaks that are converted into DSBs when encountered by a moving replication fork (*14*, *15*). In agreement with this model, we found that treatment with the challenging CPT dose alone (100 nM or 1 μM) led to an increase in DSBs by neutral comet assay (Fig. 3, D and E). However, the levels of DSBs induced by the challenging dose were significantly reduced when cells were pretreated with a low dose of CPT 24 hours before (Fig. 3, D and E). Notably, because of their inability to repair the damage, TDP1 KO cells accumulated even more DSBs upon treatment with a single CPT dose compared to WT cells. Nonetheless, treatment with the predose + challenging dose also diminished DSBs in this repair-deficient background, suggesting that other factors may be able to clear TOP1-ccs from DNA (Fig. 3, D and E). In agreement with the comet results, we also found that treatment with the predose + challenging dose lowers the levels of γ-H2AX and RAD51 foci caused by treatment with the challenging dose alone (Fig. 3F and fig. S3I). In summary, our results show that the adaptive response to CPT lowers the damage induced by the drug, and this translates into a reduction of replication stress and DNA breaks.

TOP1-cc ubiquitination mediates the adaptive response to CPT by promoting TOP1cc degradation

TOP1-ccs can be degraded through the ubiquitin-proteasome pathway (*24*, *55*, *56*). Therefore, we asked whether the adaptive response to CPT requires protein ubiquitination. To this end, we inhibited the E1 ubiquitin enzyme by using a low concentration of the specific E1 inhibitor TAK-243 (0.1 μM) (*57*). Our Western blot analysis confirmed that prolonged treatment with low concentration of TAK-243 markedly decreased the levels of ubiquitinated proteins without affecting the total levels of TOP1 protein (*57*). Ubiquitinated proteins started to reaccumulate 4 hours after inhibitor removal in both WT and TDP1 KO cells (Fig. 4A). Next, we studied whether suppressing protein ubiquitination by E1 inhibition abrogates the effect of the CPT challenging dose on replication fork progression by DNA fiber assay. TAK-243 was added 1 hour before treatment with the predose and removed 4 hours before performing the DNA fiber assay in the presence of the challenging dose (see scheme of Fig. 4B). Removing the inhibitor 4 hours before performing the DNA fiber assays partially restored protein ubiquitination (Fig. 4A), which is necessary for replication initiation and elongation (*58*). Treatment with E1 inhibitor abrogated the replication fork rescue phenotype conferred by the predose in both WT and TDP1 KO cells (Fig. 4B and fig. S4A), suggesting a role for E1 ubiquitination activity in the adaptive response to CPT.

Next, we tested whether TOP1-cc ubiquitination is specifically required for the adaptive response to CPT. The detection of TOP1-cc ubiquitination is challenging because of its transient nature and paucity with respect to the total TOP1. We optimized a protocol to specifically monitor TOP1-cc ubiquitination by SDS–polyacrylamide gel electrophoresis (SDS-PAGE) and Western blot (Fig. 4C), based on the work of Sun *et al.* (*59*). First, we extracted DNA covalently bound to TOP1-ccs using the same protocol of the RADAR assay (see Materials and Methods) (*48*). Next, we digested the DNA with micrococcal nuclease to release single nucleosomes and loaded the samples on an SDS-PAGE gel. The samples were normalized for the total DNA content as in the case of the RADAR assay. By probing with the anti-TOP1 antibody, we were able to detect a single band corresponding to unmodified TOP1 in all the samples, confirming that TOP1 was effectively pulled down in these experiments (Fig. 4D). Moreover, we were able to detect endogenous TOP1 ubiquitination as a high–molecular weight smear using the anti-ubiquitin antibody. Treatment with the challenging dose alone induced an increase in ubiquitinated TOP1-ccs, in agreement with previous findings (*24*, *55*, *56*) (Fig. 4, D and E, compare lanes 1 and 2 for WT and lanes 5 and 6 for TDP1 KO). The levels of ubiquitinated TOP1-ccs were further increased upon treatment with the predose + challenging dose (Fig. 4, D and E, and fig. S4). Notably, we were not able to detect a similar increase in ubiquitinated TOP1-ccs in TDP1 KO cells treated with multiple CPT doses. A possible explanation for these results is that treatment of TDP1 KO with a single CPT dose leads to a strong increase in the ubiquitination levels of TOP1-ccs, which might be close to the detection limit of the assay, precluding the detection of any further increase that might be caused by the addition of the predose (Fig. 4, D and E, and fig. S4B).

On the basis of previous studies showing that the proteasome regulates TOP1 and TOP1-cc levels (*56*) and considering that treatment with multiple CPT doses decreases the levels of TOP1-ccs (Fig. 2, A and B), we tested whether TOP1-cc ubiquitination promotes its proteasome-mediated degradation. To this end, we inhibited the 26*S* proteasome with a low dose of MG132 (0.5 μM) and let cells recover for 30 min after inhibitor removal (see the experimental scheme in Fig. 4F). Our Western analysis showed that both WT and TDP1 KO cells accumulate ubiquitinated proteins during this prolonged treatment with MG132 (Fig. 4F). Moreover, we found that the total ubiquitin signal did not decrease 30 min after MG132 removal. Next, we performed the DNA fiber analysis under the same experimental conditions and found that the fork slowing phenotype caused by the challenging dose alone was not rescued upon addition of the predose when cells were pretreated with MG132 (Fig. 4G and fig. S4C). These results suggest that a functional proteasome system is needed for adaptive response to CPT, likely to degrade TOP1-ccs.

The CUL3 E3 ligase complex promotes TOP1-cc ubiquitination upon treatment with multiple CPT doses

Protein ubiquitination is mediated by the conjunct action of three enzymes: the E1 ubiquitin–activating enzyme, the E2 ubiquitin–conjugating enzyme, and the E3 ubiquitin ligase enzyme that specifically binds the target protein. The technical challenge in detecting ubiquitinated TOP1 species also translates into determining the E3 ligase involved in this process. Recent studies associated two Cullin Ring E3 ubiquitin ligases, CUL3 and CUL4, with TOP1 ubiquitination (*25*, *26*). Therefore, we sought to investigate whether these two Cullins were involved in the adaptive response to CPT. We found that loss of CUL3 did not affect TOP1 total levels in WT and TDP1 KO cells (Fig. 5A) but affected their ability to adapt to treatment with multiple CPT doses. Specifically, the DNA fiber experiments showed that the replication fork rescue phenotype observed upon treatment with the predose + challenging dose was no longer detectable in cells depleted of CUL3 (Fig. 5B). We then investigated the role of CUL3 in TOP1-cc accumulation during the adaptive response to CPT by RADAR assay. We found that depletion of CUL3 prevented the reduction of TOP1-ccs caused by treatment with multiple CPT doses in both WT and TDP1 KO cells (Fig. 5, C and D, and fig. S5A for RADAR DNA loading control). In addition, we measured the ubiquitination state of TOP1-cc in the absence of CUL3 and observed that the loss of CUL3 prevented the increase of TOP1-cc ubiquitination associated with the adaptive response to CPT (fig. S5, B to D; compare lanes 6 and 8 of fig. S5B).

Two adaptor proteins, BTBD1 and BTBD2, were previously shown to mediate the interaction between TOP1 and CUL3 (*60*). Depletion of either BTBD1 or BTBD2 alone did not affect the adaptive response to CPT (fig. S5, E and F). On the other hand, the concomitant loss of BTBD1 and BTBD2 abrogated the fork rescue phenotype associated with treatment with multiple CPT doses (fig. S5G), suggesting that these two proteins play redundant roles in the adaptive response to CPT. To confirm that the interaction between BTBD1 and TOP1 is required for this response, we repeated the DNA fiber assays in BTBD1/BTBD2-depleted cells expressing a BTBD1 (ΔC) mutant that carries a deletion of 112 amino acids at the C terminus, preventing its interaction with TOP1 (Fig. 5E) (*60*). Expression of WT BTBD1 in BTBD1/BTBD2-depleted cells rescued fork progression upon treatment with the predose + challenging done (Fig. 5F, compare lanes 5 and 6). However, replication fork progression was not rescued upon expression of the BTBD1 (ΔC) mutant, confirming that the interaction between TOP1 and

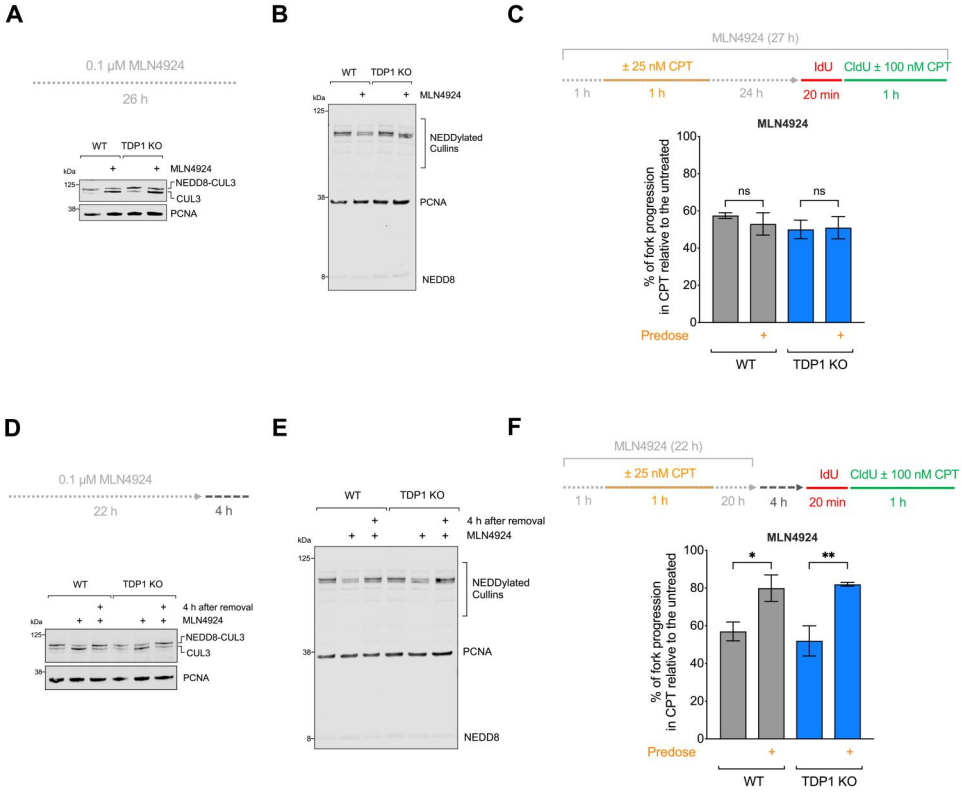

Fig. 5. The CUL3 complex promotes TOP1-cc ubiquitination. (**A**) Western blot for CUL3 and TOP1 in WT and TDP1 KO cells silenced for CUL3. (**B**) Top: Experimental scheme for the DNA fiber analysis in WT and TDP1 KO cells silenced with either siCTRL or siCUL3, ± predose (25 nM CPT), and ± challenging dose (100 nM CPT). Bottom: Mean ± SEM of % of DNA replication progression in CPT treated relative to untreated cells ($N = 3$). RM one-way ANOVA, $^{****}P \leq 0.0001$. (**C**) Top: Experimental scheme for the RADAR assay ± predose (25 nM CPT) and ± challenging dose (1 μM CPT). Bottom: Representative RADAR assay of WT TDP1 KO cells silenced with either siCTRL or siCUL3 and treated as shown in (B). (**D**) RADAR assay quantification of TOP1-ccs; values are normalized with respect to the untreated WT control and plotted as TOP1-cc fold change mean ± SEM ($N = 3$). RM one-way ANOVA, $^{*}P \leq 0.05$, $^{**}P \leq 0.01$, and $^{****}P \leq 0.0001$. (**E**) Western blot for BTBD1 in cells silenced for BTBD1 and BTBD2 and overexpressing either BTBD1-WT or BTBD1-ΔC mutant. (**F**) Mean ± SEM of % of DNA replication progression in CPT relative to untreated WT cells silenced either with siCTRL or siBTBD1 and siBTBD2 and complemented with either BTBD1-WT or BTBD1-ΔC mutant ($N = 3$). RM one-way ANOVA, $^{***}P \leq 0.001$ and $^{****}P \leq 0.0001$.

BTBD1 is crucial for the adaptive response to CPT (Fig. 5F, compare lanes 7 and 8).

Next, we depleted Cullin 4 (CUL4A and CUL4B) to test whether the observed phenotype was specific for CUL3 or shared by other Cullins. However, loss of Cullin 4 led to a significant decrease in the rates of replication progression even in untreated cells, precluding a proper evaluation of its role in the adaptive response to CPT (fig. S5H). On the basis of recent findings that TOP1-ccs can be ubiquitylated by RNF4 after SUMOylation (*59*), we also tested whether loss of RNF4 affects the adaptive response to CPT. Our data show that RNF4 is not involved in this adaptive process, suggesting that SUMOylation of TOP1-cc is not necessary for adaptation (fig. S5, I and J). Collectively, our findings suggest that a pathway mediated by CUL3, and its adaptor proteins BTBD1 and BTBD2, controls the adaptive response to CPT by promoting TOP1-cc ubiquitination and degradation.

NEDDylation regulates the CUL3-dependent adaptive response to CPT

NEDDylation is a ubiquitin-like posttranslational modification pathway, and specific E1, E2, and E3 enzymes collaborate to conjugate the NEDD8 molecule on protein targets (*61*). NEDD8 is a small peptide, very similar to ubiquitin that regulates protein function or interaction. NEDDylation is a poorly studied posttranslational modification that is gaining attention for its regulatory role in the DNA damage response (*62*, *63*) and was implicated in the regulation of Cullins (*64*–*66*). We used the specific NEDD8 E1–activating enzyme inhibitor pevonedistat (MLN4924) to study the role of NEDDylation in the adaptive response to CPT (*67*, *68*). First, we treated WT and TDP1 KO cells with MLN4924 (0.1 μM) for 26 hours and verified that treatment with this low dose of MLN4924 inhibits CUL3 NEDDylation by Western blot (Fig. 6A). We confirmed that treatment with MLN4924 reduced the ratio between the higher molecular weight band of CUL3, corresponding to the NEDDylated CUL3 (*69*), and the lower band, corresponding to unmodified CUL3, in both cell lines (Fig. 6A). In addition, we monitored the total NEDDylation levels with an anti-NEDD8 antibody and confirmed that treatment with the MLN4924 inhibitor reduces the total levels of NEDDylation, which mostly come from NEDDylated Cullins (Fig. 6B) (*70*, *71*). By DNA fiber analysis, we found that inhibition of NEDDylation throughout the entire duration of the multiple-dose experiment abrogated the adaptive response to CPT (Fig. 6C and fig. S6A). We found that the effect of NEDDylation inhibitor was completely reversible after 4 hours of removal because the levels of CUL3 NEDDylation and total NEDDylation were fully restored at this time point (Fig. 6, D and E). We then performed a DNA fiber assay, removing the NEDDylation inhibitor 4 hours before thymidine labeling. Under these experimental conditions, we found that addition of the predose with the challenging dose was able to rescue CPT-induced fork slowing in both WT and TDP1 KO (Fig. 6F and fig. S6B). On the basis of these results, we propose that CUL3 NEDDylation is critical for the adaptive response to CPT and that cells can adapt to treatment with multiple CPT doses only if CUL3 NEDDylation is restored before treatment with the challenging dose.

Loss of CUL3 or NEDD8 inhibition increases cancer cell sensitivity to CPT

Irinotecan and topotecan are CPT analogs widely used for cancer treatment (*6*, *7*). We asked whether these two analogs trigger the same adaptive response observed with CPT. We used two concentrations of irinotecan and topotecan that are comparable to the CPT doses used in our previous experiments, based on the median inhibitory concentration (IC_{50}) values previously reported for these TOP1 inhibitors (*72*, *73*). To our knowledge, there is no available information on the actual concentration of TOP1 inhibitors present in tumor cells in vivo. However, the nanomolar concentrations of irinotecan and topotecan used in our experiments closely reflect the concentrations derived from the peak plasma levels of patients treated with these two drugs (*74*–*77*). We found that treatment with the challenging dose alone of either analog induced replication slowing, and this was rescued by addition of the predose (Fig. 7A and fig. S7A). The challenging dose also led to the accumulation of TOP1-ccs, which was significantly lowered upon addition of the predose (Fig. 7, B and C, and fig. S7B for RADAR DNA loading control), confirming that the adaptive response is activated following treatments with these clinically relevant CPT analogs.

Next, we tested whether treatment with a combination of CPT and CUL3 small interfering RNAs (siRNAs), MLN4924, or both affects cell viability in U2OS and colon cancer cells (RKO), as a model of cancer that is often treated with CPT analogs (*78*–*81*). Our MTS assays showed that addition of MLN4924 or CUL3 depletion significantly increased cancer cell sensitivity to CPT (Fig. 7, D and E, and fig. S7, C and D). There was no further sensitization to CPT when CUL3-depleted cells were treated with MLN4924, supporting the notion that CUL3 and NEDD8 work in the same pathway (Fig. 7, D and E). Together, the data indicate that CUL3 and NEDD8 play an important role in modulating the adaptive response to CPT and can be exploited for combinational therapies in tumors.

DISCUSSION

DNA TOP1 inhibitors are widely used as anticancer drugs that act by trapping the topoisomerase on DNA, resulting in the stabilization of TOP1-ccs. The accumulation of these bulky TOP1-ccs perturbs DNA replication and transcription, ultimately leading to DNA breaks and cell death. Here, we studied how cells adapt to treatment with multiple CPT doses. Cellular adaptation is the process by which cells adapt to treatment with low doses of genotoxic stress and optimize their response to subsequent treatments with the same genotoxic agent. Understanding how cells adapt to multiple drug doses has become increasingly important in the context of cancer treatment where patients are treated with multiple rounds of chemotherapeutics. This process has been initially investigated in cells treated with multiple rounds of x-ray radiation and oxidative stress (*32*–*37*, *82*) and more recently extended to cells treated with platinum-based compounds (*38*). However, little is known about the mechanisms of cellular adaptation to other genotoxic agents, including DNA TOP1 inhibitors, and mechanistic insights into how multiple-dose regimens affect the DNA replication stress response are lacking.

Our data show that cells adapt to treatment with multiple CPT doses by activating a molecular pathway that promotes the

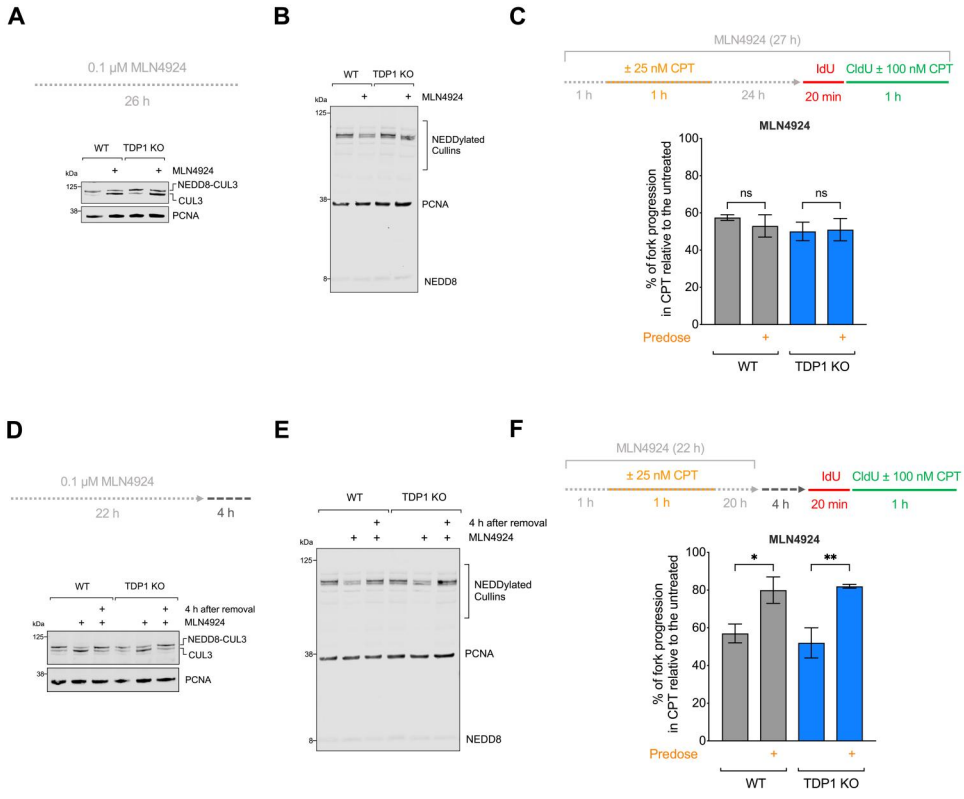

Fig. 6. CUL3 NEDDylation controls the adaptive response to CPT. (**A**) Top: Experimental scheme for MLN4924 inhibition. Bottom: Western blot of CUL3 in WT and TDP1 KO cells treated with 0.1 μM MLN4924 for 26 hours. The higher molecular weight band represents the NEDDylated Cullin3 (NEDD8-CUL3), and the lower band represents the nonmodified CUL3. (**B**) Western blot of total NEDDylated Cullins and NEDD8 detected by anti-NEDD8 antibody. WT and TDP1 KO cells are treated according to the scheme in (A). (**C**) Top: Experimental scheme for the DNA fiber assay with MLN4924 ± predose (25 nM CPT) and ± challenging dose (100 nM CPT). MLN4924 (0.1 μM) was added 1 hour before the predose and kept for the entire duration of the experiment. Bottom: Mean ± SEM of % of DNA replication progression in CPT treated relative to untreated cells ($N = 2$). RM one-way ANOVA. (**D**) Western blot of CUL3 in WT and TDP1 KO cells treated with 0.1 μM MLN4924 and 4 hours after its removal, as shown in the experimental scheme on top. (**E**) Western blot of total NEDDylated Cullins and NEDD8, both detected by anti-NEDD8 antibody, treated according to the scheme in (D). (**F**) Top: Experimental scheme for the DNA fiber assay after MLN4924 removal ± predose (25 nM CPT) and ± challenging dose (100 nM CPT). MLN4924 (0.1 μM) was added 1 hour before the predose and removed 4 hours before the DNA fiber assay. Bottom: Mean ± SEM of % of DNA replication progression in CPT treated relative to untreated WT and TDP1 KO cells ($N = 2$). RM one-way ANOVA, $*P \leq 0.05$ and $**P \leq 0.01$.

degradation of TOP1-ccs, thereby allowing cells to better tolerate subsequent doses of CPT, as well as other TOP1 inhibitors. This adaptive response pathway is mediated by the E3-RING CUL3 ligase and the BTBD1 and BTBD2 adaptor proteins, which promote TOP1 ubiquitination and its subsequent proteasomal degradation (Fig. 8). NEDDylation of CUL3 is essential to activate this pathway, and inhibiting protein NEDDylation sensitizes cancer cells to TOP1 inhibitors (Fig. 8). This pathway selectively targets TOP1-ccs bound to chromatin, but it does not cause a reduction in the total TOP1 protein levels, which would otherwise lead to increased genomic instability (*83*, *84*) and transcriptional dysregulation (*85*, *86*). This might result in a higher fraction of TOP1 bound on the DNA (or localized in the vicinity of DNA, perhaps as part of a protein complex) (*39*, *85*) but not covalently engaged with the DNA. The activation of this TOP1-cc degradation pathway increases tolerance to subsequent doses of TOP1 inhibitors by reducing replication perturbations and accumulation of DNA breaks that would normally originate from the collision of replication forks with TOP1-ccs. Our fork asymmetry data argue that CPT interferes with the progression of preexisting replication forks that fired before CPT treatment because treatment with the challenging CPT dose leads to a marked decrease in the percentage of symmetric forks relative to untreated cells. Thus, an interesting avenue for future studies would be to investigate whether the replication perturbations caused by CPT treatment cause a more global effect on fork progression, not necessarily restricted to sites of replication fork barriers, as recently proposed in the case of interstrand crosslinks (*87*).

Our previous studies showed that BRCA1-deficient cancer cells adapt to multiple rounds of cisplatin treatment by up-regulating repriming by PRIMPOL. This mechanism allows replication forks to skip the cisplatin-induced lesions and resume DNA synthesis downstream of the lesions (*38*). In this work, we found that the repriming pathway is not responsible for the reduced replication fork perturbations observed upon treatment with multiple doses of TOP1 inhibitors, suggesting that cells activate different adaptive response mechanisms to deal with distinct types of replication challenges.

Many factors are involved in TOP1-cc repair and removal (*19*), but how these factors are regulated is still unclear. We have found

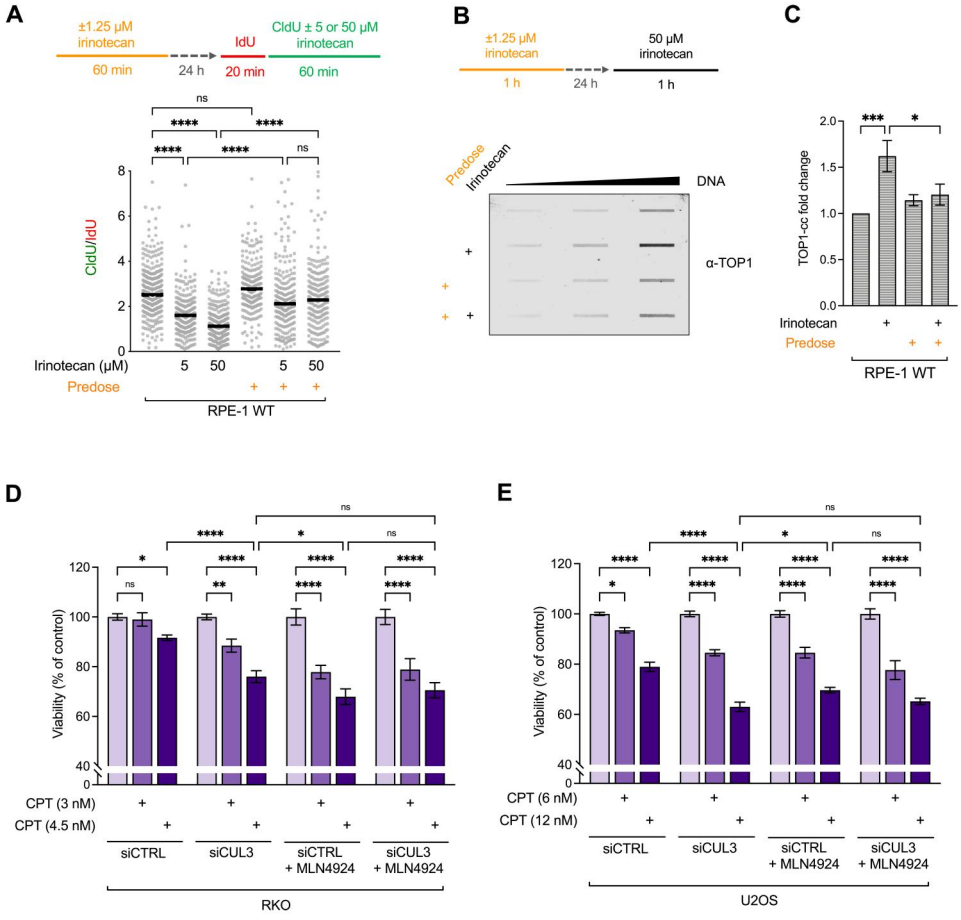

Fig. 7. Loss of CUL3 or NEDD8 inhibition sensitizes cancer cells to low CPT doses. (**A**) Top: Experimental scheme for the DNA fiber assay. Bottom: Dot plot and median of CldU/IdU ratio in WT cells treated ± irinotecan predose (1.25 μM) ± irinotecan challenging dose (5 or 50 μM) added 24 hours after the predose ($N = 2$). RM one-way ANOVA, $^{****}P \leq 0.0001$. (**B**) Top: Experimental scheme for the RADAR assay ± irinotecan predose (1.25 μM) ± irinotecan challenging dose (50 μM). Bottom: Representative RADAR assay to measure Top1-covalent complexes in WT cells. (**C**) RADAR assay quantification of TOP1-ccs; values are normalized relative to the untreated WT control and plotted as TOP1-cc fold change mean ± SEM ($N = 3$). RM one-way ANOVA, $^{*}P \leq 0.05$ and $^{***}P \leq 0.001$. (**D** and **E**) Viability assay of RKO and U2OS cells treated with a combination of CPT and siCTRL, siCUL3, MLN4924, or both. Viability is measured by MTS assay and expressed as a % of the respective untreated control ($N = 4$). RM one-way ANOVA, $^{*}P \leq 0.05$ and $^{****}P \leq 0.0001$.

that the adaptive response to CPT can occur in the absence of TDP1, a key factor necessary to cleave the covalent bound between TOP1 and the DNA (*21*–*23*). We speculate that in the absence of TDP1, other factors might cleave the covalent bond between TOP1 and DNA after TOP1 has been degraded by the proteasome. For example, MRE11 and CtIP (*88*, *89*), XPF-ERCC1 (*90*, *91*), and SLX4-SLX1 (*92*) have been implicated in the cleavage of stable TOP1-ccs and might play a more prominent role in the absence of TDP1.

We also found that the CUL3 E3 ligase is essential for this pathway in both WT and TDP1 KO cells. Cullins are the most abundant family of cellular E3 ligases and serve as a scaffold to form a functional E3 complex together with RING proteins and specific adaptors (*93*). There are seven different Cullins, all with their own specific complex composition and substrate targets. CUL3 is frequently overexpressed in cancer, and its overexpression has been linked to increased TOP1 ubiquitination (*25*). Moreover, overexpression of CUL3 was specifically linked to cancer cell resistance to CPT treatment (*25*). CUL4 includes two proteins named Cullin 4A and Cullin 4B, which share 80% identity. A mutation in the Cullin 4B gene has been reported to abolish CPT-dependent ubiquitination of TOP1 (*26*), whereas Cullin 4A was shown to be enriched at CPT-challenged replication forks by Isolation of Proteins on Nascent DNA mass spectrometry (*94*). Our data show that CUL3 is essential to promote increased TOP1-cc ubiquitination and degradation and to rescue replication fork progression after treatment with multiple CPT doses. On the basis of a previous study suggesting that adaptor proteins, BTBD1 and BTBD2, mediate the interaction between TOP1 and CUL3 (*60*), we also confirmed that the interaction between BTBD1 and TOP1 is essential for the adaptive response to CPT. Unfortunately, we were not able to properly evaluate the function of CUL4 within the same adaptive response pathway because loss of CUL4 affects replication fork progression even in unperturbed conditions. These findings suggest that CUL4 might play a previously unappreciated role during DNA replication fork progression, which deserves further investigation.

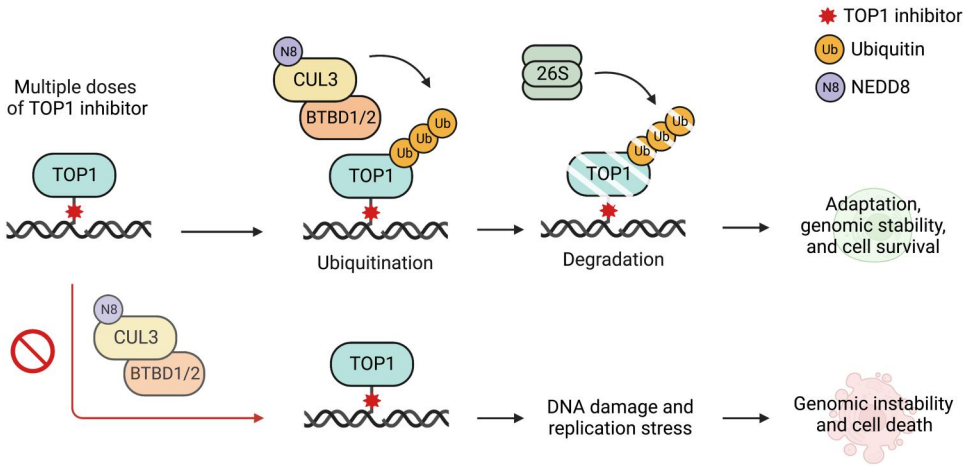

Fig. 8. Model for the adaptive response to TOP1 inhibitors. The CUL3-BTBD1/BTBD2 complex is activated by NEDD8 conjugation and ubiquitinates TOP1-covalent complexes to promote their degradation. As a result, TOP1-cc accumulation is reduced, decreasing DNA breaks and replication stress, and promoting genomic stability and cell survival. Inhibition of the NEDD8 pathway or loss of the CUL3-BTBD1/BTBD2 complex limits the removal of TOP1-ccs, increasing DNA damage and replication perturbations, and promoting genomic instability and cell death.

Recent studies showed that TOP1-ccs can be SUMOylated, and this modification serves as a signal for SUMO-targeted ubiquitin ligases (STUbLs) including RNF4, which ubiquitinate TOP1 to promote proteasomal degradation (*59*). Our data suggest that RNF4 is not involved in the adaptive response to CPT. However, this result does not rule out the possibility that alternative SUMO-targeted ligases might be involved in this process. Moreover, nonproteasomal proteases, such as SPRTN (*31*, *95*, *96*) and FAM111A (*97*), are able to cleave TOP1-ccs in mammalian cells. Future studies would be necessary to test whether these proteases contribute to the adaptive response to TOP1 inhibitors and whether there is a cross-talk between the different TOP1-cc degradation pathways. An interesting avenue for future studies would also be to determine whether the activation of these different pathways is dependent on the genomic location of the damage or the chromatin context.

Defining adaptive response mechanisms is paramount to understanding how cancer cells adapt to chemotherapy and to identifying potential targets for cancer treatment. We found that loss of CUL3 enhances cancer cell sensitivity to low doses of TOP1 inhibitors. CUL3 is regulated by NEDDylation, a posttranslational modification similar to ubiquitin (*64*, *66*, *69*, *93*). In agreement with these findings, we also show that inhibition of the NEDDylation pathway with the NEDD8 inhibitor, pevonedistat (MLN4924), completely abrogates the adaptive response to TOP1 inhibitors and significantly sensitizes cancer cells to these drugs. Pevonedistat is currently in clinical trials for the treatment of different tumor types (*98*–*100*), and our data strongly suggest that this drug can be used to increase tumor response to TOP1 inhibitors.

In summary, our findings uncover a previously unidetified pathway mediated by NEED8, the E3-RING CUL3 ligase, and the BTBD1 and BTBD2 adaptor proteins, which promote the removal of TOP1 bound to DNA through its ubiquitination in response to treatment with DNA TOP1 inhibitors. Combined with previous studies performed with x-ray and UV radiation (*37*, *82*), oxidative stress inducers (*34*), and platinum-based compounds (*38*), our work strengthens the idea that cells have evolved different adaptive response mechanisms depending on the type of stress they encounter. While recent research focused on the models of established drug resistance, the investigation of early adaptive response mechanisms to genotoxic stress is still in its infancy. We propose that studying these mechanisms can provide invaluable information for the design of novel targeted cancer therapies and broaden our understanding of the molecular steps of adaptation that might contribute to the development of drug resistance.

MATERIALS AND METHODS

Cell culture and cell lines

Retinal pigmented epithelial cells immortalized with hTERT RPE-1 and TDP1 KO RPE-1 (provided by K. Caldecott, Sussex, UK) were grown in Dulbecco's modified Eagle's medium (DMEM) F12 (Gibco), RKO colorectal cancer cells (provided by E. Sherif, UK) were grown in RPMI 160 medium, and human osteosarcoma U2OS cells (American Type Culture Collection) were grown in DMEM, all supplemented with 10% fetal bovine serum, penicillin (100 U/ml), and streptomycin (100 mg/ml), at 37°C, 5% CO_2.

TOP1 ChIP-seq

TOP1 ChIP was performed on RPE-1 cells as described previously (*101*) with minor modifications. Briefly, after treating with the challenging dose, cells were treated for 5 min with 1 μM CPT to increase the probability to trap TOP1 on the DNA. Cells were cross-linked with 1% formaldehyde (Thermo Fisher Scientific, 28906) for 5 min. Cross-linking was stopped by the addition of 125 mM glycine (Sigma-Aldrich, 50046), and cells were washed twice with cold phosphate-buffered saline (PBS). After harvesting cells, the pellet was washed once with PBS plus 0.5% bovine serum albumin (BSA) and resuspended in TE-SDS 0.1% [10 mM tris-HCl (pH 8.0), 1 mM EDTA (pH 8.0), 0.1% SDS] with complete protease inhibitor tablet (Roche) to a final concentration of 1×10^7 cells/ml. Samples were sonicated with a Bandelin probe sonicator (30% amplitude, four times, 30″ ON/30″ OFF) and then with a Covaris ME220 sonicator for 10 min using the 1-ml High Cell protocol

(peak power: 75; duty % factor: 15; cycles/burst: 1000; average power: 11.25) to produce chromatin fragments of 200 to 500 base pairs (bp) on average. After centrifugation, sonicated extracts were adjusted to the conditions of radioimmunoprecipitation assay (RIPA) buffer [10 mM tris (pH 8.0), 1 mM EDTA (pH 8.0), 1% Triton X-100, 0.1% SDS, 200 mM NaCl, and 0.1% Na-deoxycholate]. Two micrograms of anti-TOP1 (ab109374) was mixed with 30 μl of protein A/G magnetic beads (Pierce, 88803) and incubated at 4°C for 6 hours with rotation. Chromatin from 10×10^6 cells was added to the protein A/G-antibody complexes and incubated overnight at 4°C with rotation. Immunoprecipitates were washed twice with RIPA buffer [10 mM tris-HCl (pH 8.0), 1 mM EDTA (pH 8.0), 1% Triton X-100, 0.1% Na-deoxycholate, 0.1% SDS, and 200 mM NaCl], twice with RIPA buffer plus 300 mM NaCl, twice with LiCl buffer [10 mM tris-HCl (pH 8.0), 1 mM EDTA (pH 8.0), 250 mM LiCl, 0.5% NP-40, and 0.5% Na-deoxycholate], and twice with TE. The beads were then resuspended in 125 μl of TE plus 0.5% SDS supplemented with proteinase K (500 μg/ml; Thermo Fisher Scientific, 25530049) and incubated overnight at 65°C. The DNA was recovered from the eluate using the QIAquick polymerase chain reaction (PCR) purification kit and finally dissolved in tris-HCl (pH 8.5). All ChIP-seq experiments were performed in duplicates.

Library preparation of ChIP samples and sequencing

DNA from ChIP were quantified with the Qubit dsDNA HS Assay Kit. Sequencing libraries were created according to the ThruPLEX DNA-seq kit protocol (Takara, R400676). Size selection was performed in the range of 200 to 700 bp with AMPure XP beads (Beckman Coulter, A63880) and confirmed using the Agilent High Sensitivity DNA Kit (Agilent, 5067-4626) on the Agilent 2100 Bioanalyzer. Libraries were pooled and sequenced using NextSeq 500/550 High Output Kit v2.5 (Illumina, 20024906). The sequencing run was Single End and Dual Index with 75-bp reads.

Gene silencing with RNA interference

Transient gene depletions were carried out using the Lipofectamine RNAiMax transfection reagent (Life Technologies), according to the manufacturer's instructions. The following siRNAs are used at a final concentration of 20 nM: ON-TARGETplus SMARTpool (Horizon) siRNA L-010224-00-0005 for CUL3, L-014617-00-0005 for BTBD1, L-016110-00-0005 for BTBD2, L-006557-00-0005 for RNF4, GCCGGAUCUGAAAAAUAAC for RAD18 at 50 nM (*102*), UAUCUAGUGAGUCUUCUCUAAACGG for CUL4A, and AAGCCUAAAUUACCAGAAATT for CUL4B at 50 nM (*26*).

Silencer select negative control #1 siRNA (4390843, Ambion) was used as control siRNA at the same concentration of the most concentrated siRNA used in the same experiment. Experiments were performed starting at 48 hours after transfection.

BTBD1-WT or BTBD1-ΔC coding sequences were cloned into a pcDNA3.1 vector (GenScript). Plasmid transfection was conducted with the Trans-IT reagent (Mirus), according to the manufacturer's instructions. Concomitant endogenous BTBD1 and BTBD2 silencing was performed with 50 nM siRNAs targeting the 3′ untranslated region of BTBD1 (UGAAAUUGCUAAAGGGAAAUU) and BTBD2 (AGACAAUCCCUCAGGACUAUU) 6 to 8 hours before transfection with the plasmids.

Drugs and cell treatments

The following drugs were used throughout the study: CPT (S1288, Selleckchem), TAK-243 E1 ubiquitin–activating enzyme inhibitor (S8341, Selleckchem), MG132 26*S* proteasome inhibitor (S2619, Selleckchem), and MLN4924 Nedd8-activating enzyme inhibitor pevonedistat (S7109, Selleckchem).

Cell cycle analysis

Cell cycle analysis and S-phase cell labeling were performed using the Click-iT EdU Imaging Kit (C10337, Invitrogen) according to the manufacturer's protocol. S-phase cells were labeled with 10 μM 5-ethynyl-2′-deoxyuridine (EdU; E10187, Thermo Fisher Scientific) for 1 hour. Cells were collected and fixed in 2% paraformaldehyde 20 min. Fixed cells were blocked in 1% BSA in PBS at room temperature (RT) for 10 min before permeabilization by 0.5% saponin in the dark for 30 min at RT. Permeabilized cells were then incubated with the Click-iT cocktail in the dark for 30 min, and the total DNA was stained with 4′,6-diamidino-2-phenylindole (DAPI) solution [1% BSA in PBS, ribonuclease A (RNase A; 0.1 mg/ml), and DAPI (2 μg/ml)] for 30 min. Samples were run through a CytoFLEX flow cytometer (Beckman Coulter), and data were analyzed and visualized using FlowJo software.

Cell viability and apoptosis analysis

Apoptotic cells were stained using the FITC (fluorescein isothiocyanate) Annexin V Apoptosis Detection Kit (88-8005-72, Thermo Fisher Scientific) according to the manufacturer's instructions. Dead cells were stained using DAPI. Samples were immediately run through a CytoFLEX flow cytometer (Beckman Coulter) and analyzed with CytExpert Analysis software. Cells treated for 24 hours with 5 μM CPT were used as a positive control in every experiment (*103*).

DNA fiber assay

DNA fiber assay was performed as previously described (*52*). Exponentially growing cells were pulse-labeled with 20 μM IdU (Millipore Sigma) for 20 min, washed three times with PBS, and then pulse-labeled with 100 μM CldU (Millipore Sigma) for 1 hour with the addition of CPT when indicated. Cells were then washed twice with PBS, collected by trypsinization, resuspended in PBS for a final concentration of 1500 cells/μl, and spotted onto positively charged glass slides. Cells were mixed with lysis buffer [200 mM tris-HCl (pH 7.5), 50 mM EDTA, and 0.5% SDS in water] and incubated for 5 min at RT, and slides were tilted at a 20° to 45° angle to spread the fibers at a constant, low speed. After 10 min of air drying, DNA was fixed onto the slides with a freshly prepared solution of methanol:glacial acetic acid at 3:1 for 5 min, dried, and then stored at 4°C for at least overnight.

For immunostaining of DNA fibers, DNA was rehydrated in PBS twice for 5 min and then denatured with 2.5 M HCl for 1 hour at RT. Slides were then washed with PBS three times and blocked with 5% BSA at 37°C for 45 min. DNA fibers were immunostained with rat anti–5-bromo-2′-deoxyuridine (BrdU) (1:75; Ab6326, Abcam, RRID: AB_305426) and mouse anti-BrdU (1:20; 347580, BD Biosciences, RRID: AB_400326) for 1.5 hours at RT, washed three times with PBS–0.05% Tween 20 for 5 min, and then incubated with anti-rat Alexa Fluor 488 and anti-mouse Alexa Fluor 546 or 568 (1:100; A-21470, A-21123, and A-21124, respectively, Thermo Fisher Scientific) for 1 hour at RT. After three washes with PBS–0.05% Tween

20 of 5 min each, slides were mounted with ProLong Gold Antifade Reagent (P36930, Thermo Fisher Scientific).

Images were acquired with LAS AF software using a Leica TCS SP5 confocal microscope and a Leica DMi8 confocal microscope with either a 63×/1.4 or 40×/1.15 oil immersion objective. Between 100 and 200 fibers per sample were measured with the ImageJ software (RRID: SCR_003070).

DNA replication progression in CPT was assessed either by plotting the CldU/IdU ratio for each individual fiber or by plotting the mean ratio between the median CldU/IdU value of CPT-treated and untreated samples from independent experiments and expressed as a % of the untreated.

S1 nuclease DNA fiber assay

The DNA fiber assay with the ssDNA-specific S1 nuclease was performed as previously described (*52*). Briefly, after analog incorporation, cells were permeabilized with CSK100 [100 mM NaCl, 10 mM Mops (pH 7), 3 mM $MgCl_2$, 300 mM sucrose, and 0.5% Triton X-100 in water], treated with the S1 nuclease (18001-016, Thermo Fisher Scientific) at 20 U/ml in S1 buffer [30 mM sodium acetate (pH 4.6), 10 mM zinc acetate, 5% glycerol, and 50 mM NaCl in water] for 30 min at 37°C, and collected in PBS–0.1% BSA with a cell scraper. Nuclei were then pelleted at ~4600*g* for 5 min at 4°C, resuspended in PBS, and processed as intact cells in the standard DNA fiber assay.

Reverse transcription PCR and primers

Total RNA was extracted using the PureLink RNA Mini Kit (12183018A, Thermo Fisher Scientific), cDNA was synthesized by M-MLV Reverse Transcriptase (28025013, Thermo Fisher Scientific), and reverse transcription PCR (RT-PCR) was performed using iQ SYBR Green Supermix (1708880, Bio-Rad) with the QuantStudio Real-Time PCR System. The primers were designed to anneal only on gene exons. The results were calculated according to the 2−ΔΔCt methodology and are shown as relative expressions to the correspondent control.

The following primers were used to verify siRNA depletions: RAD18-F 5′-ACCGCATATTAGATGAACTGGTAA-3′ and RAD18-R 5′-AGAGGAAGAAGCAGGAGATTT-3′; BTBD1-F 5′-CCGGTTCCCACTGATGACAA-3′ and BTBD1-R 5′-GACAGCATCTTGGTCGGTCA-3′ and/or BTBD1-F2 5′-GGCGCTGCTGAGATTTCTAT-3′ and BTBD1-R2 5′-GCTGGGACTGCGTATTTCTT-3′; BTBD2-F 5′-TCCTCGCACTGCTCAAGTTT-3′ and BTBD2-R 5′-GGCTCGCAGGTTCTTCTTCA-3′; RNF4-F 5′-TTCCCTGCAAACCTTGGTATAG-3′ and RNF4-R 5′-GAGTTCGCTTCTGAGCTTGT-3′.

Western blot

Cells were collected by centrifugation, resuspended in lysis buffer [50 mM tris-HCl (pH 7.5), 20 mM NaCl, 1 mM $MgCl_2$, 0.1% SDS, 1× protease inhibitor, benzonase, 71206, Novagen], and incubated on ice for 30 min. The extract was then clarified with high-speed centrifugation, and the total protein concentration was measured using a Pierce BCA protein assay kit (23227, Thermo Fisher Scientific) according to the manufacturer′s instructions. The 1× NuPAGE LDS sample buffer (NP0007, Thermo Fisher Scientific) and the 10× sample reducing agent (NP0004, Thermo Fisher Scientific) were added to the samples, and then they were denatured at 95°C for 5 min. Approximately 10 to 25 μg of proteins were loaded onto a NuPAGE Novex 4 to 12% bis-tris gel (NP0322BOX, Thermo Fisher Scientific) and run with 1× NuPAGE MES SDS Running buffer (NP0002, Thermo Fisher Scientific) at 200 V. Proteins were transferred onto a 0.45-μm pore nitrocellulose membrane (10600002, GE Healthcare Life Sciences) by cold wet transfer in 1× tris/glycine buffer (1610734, Bio-Rad) and 20% methanol at a constant of 400 mA for 45 min. Membranes were blocked with 3% milk (170-6404, Bio-Rad) in Tris-Buffered Saline with Tween 20 (TBS-T) 0.1% for 1 hour at RT and probed with primary antibodies overnight (*104*). The following primary antibodies were used: mouse TOP1 (1:500; C-21, 556597, BD Biosciences), rabbit TOP1 (1:2000; ab28432, Abcam, RRID:AB_778545), CUL3 (1:500; PA5-17397, Thermo Fisher Scientific, RRID:AB_10985263), CUL4A (1:1000; 2699, Cell Signaling, RRID:AB_2086563), CUL4B (1:1000; 60151-1-Ig, Proteintech, RRID:AB_10641034), NEDD8 (1:1000; 2754, Cell Signaling, RRID:AB_10695300), Tdp1 (1:1000; ab4166, Abcam, RRID:AB_304337), total ubiquitin (1:5000; MAB8595, R&D Systems), BTBD1 (1:500; 15859-1-AP, Proteintech, RRID:AB_2067248), γ-H2AX (1:1000; 05-636, Millipore, RRID:AB_309864), H2AX (1:1000; 2595S, Cell Signaling, RRID:AB_10694556), PCNA (1:5000; PC10 ab29, Abcam, RRID:AB_303394), glyceraldehyde-3-phosphate dehydrogenase (GAPDH) (1:20,000; ab181602, Abcam, RRID:AB_2630358), and H3 (1:10,000; ab1791, Abcam, RRID:AB_302613). Membranes were developed with the Odyssey CLx machine (LI-COR) by incubation with secondary infrared antibodies IRDye 800CW and 680RD (925-32210 and 925-68071, LI-COR). Images were processed with ImageStudio Software (LI-COR, RRID: SCR_013715).

RADAR assay

RADAR protocol was performed as described (*48*). Cells (4.5×10^5) were seeded in six-well plates and then treated according to the experimental scheme. After CPT treatment, the medium was removed, and cells were lysed with 1 ml of DNAzol (10503027, Thermo Fisher Scientific) and collected by scraping. Genomic DNA and DNA-protein covalent complexes were precipitated at −20°C by addition of 0.5 volume of 100% cold ethanol, recovered by centrifugation at 10000 rpm at 4°C, washed twice in 70% ethanol, and resuspended in 300 μl of freshly prepared 8 mM NaOH after air drying for 3 min. The DNA content was measured with a NanoDrop One instrument (Thermo Fisher Scientific), normalized in 1 ml of tris-buffered saline buffer at 10 ng/μl, and measured again before starting with the slot blotting procedure. DNA was then deposited onto a 0.45-μm nitrocellulose membrane (Amersham) using a slot blotting apparatus (1706542, Bio-Rad). TOP1-ccs were detected by overnight incubation with primary rabbit anti-TOP1 antibody (1:2000; ab28432, Abcam, RRID:AB_778545) and secondary IRDye 800CW goat anti-mouse immunoglobulin G (926-32210, LI-COR). Images were acquired with Odyssey CLx Imager (LI-COR), and TOP1-ccs were quantified by ImageStudio Software (RRID: SCR_013715) and are expressed as fold change normalized on the untreated WT sample.

TOP1-cc ubiquitination assay

Samples were prepared following the RADAR assay protocol (*48*) and resuspended in 120 μl of freshly prepared 8 mM NaOH. The recovered DNA-protein covalent complexes were heated for 15

min at 65°C. Forty microliters of each sample were transferred into a new tube and digested with 50 U of micrococcal nuclease (Thermo Fisher Scientific) and RNase A (100 μg/ml; Thermo Fisher Scientific), in the presence of 5 mM $CaCl_2$, at 37°C for 15 min. Reactions were stopped by adding 20 mM final concentration of EDTA/NaOH and by keeping them on ice. The DNA content was quantified with a NanoDrop One instrument (Thermo Fisher Scientific), normalized at 380 ng/μl, and quantified again before addition of NuPAGE LDS 4× sample buffer (Thermo Fisher Scientific) and 10× reducing agent (Thermo Fisher Scientific). Samples were boiled for 10 min at 70°C and loaded onto 10% NuPAGE Bolt Gels at 165 V. Proteins were wet-transferred onto polyvinylidene difluoride membrane with the NuPAGE Mini Blot Module (B1000), according to the manufacturer′s instructions. Membranes were blocked with 3% milk (170-6404, Bio-Rad) in 0.1% TBS-T for 1 hour at RT, probed with anti-ubiquitin antibody overnight (1:5000; MAB8595, R&D Systems), and developed with the Odyssey CLx machine (LI-COR) by incubation with secondary infrared antibodies IRDye 800CW (925-68071, LI-COR). Images were processed with Image-Studio Software (LI-COR, RRID: SCR_013715). The entire smeared band generated by the ubiquitin signal was considered to quantify the levels of TOP1-cc ubiquitination. The values are then plotted as relative to the WT untreated condition.

Cell viability assay

Cell viability was assessed using the CellTiter 96 AQueous Non-Radioactive Cell Proliferation Assay (MTS, G5421, Promega) according to the manufacturer′s instructions. Cells (1500 to 3000 per well) were seeded in quadruplicate in a 96-well plate, and then they were treated with the indicated concentration of drugs for 4 to 5 days. MTS values were read with EnVision 2103 Multilabel Reader (PerkinElmer) with the Envision Manager software version 1.13.3009.1409. Viability was calculated and expressed as percentage with respect to each untreated control.

Neutral comet assay

Neutral comet assay was performed according to the Trevigen Comet Assay protocol (*105*). Cells were collected and resuspended in 1% low-melting agarose (Trevigen, 4250-50-050-02), spread onto a comet slide (Trevigen, 4250-200-03), and allowed to dry. Cells were then lysed in lysis solution (Trevigen, 4250-050-01) at 4°C for 1 hour. Slides were immersed in TBE buffer (0.1 M tris base, 0.1 M boric acid, and 2.5 mM EDTA) for 30 min before electrophoresis at 25 V for 30 min at 4°C. DNA was precipitated with 1 M ammonium acetate in 95% ethanol for 30 min and subsequently fixed in 70% ethanol for 30 min. Comets were stained with SYBR Gold (Thermo Fisher Scientific) for 30 min. Images were acquired with a Leica DM4B microscope with 10× objective. At least 150 comets were scored for each sample using the OpenComet plugin in the ImageJ analysis software (RRID: SCR_003070). Olive moment values are represented as Tuckey boxes.

Immunofluorescence

Cells were pre-extracted with 0.5% Triton X-100 in PBS for 5 min on ice, followed by fixation with 4% paraformaldehyde for 15 min at RT. Next, cells were permeabilized with 0.5% Triton X-100 in PBS for 5 min and washed with 0.2% PBS-T (Tween 20) three to four times. After blocking with BSA, coverslips were incubated with the following antibodies: rat BrdU antibody (1:200; ab6326, Abcam, RRID:AB_305426) for CldU foci detection and rabbit RAD51 (1:250; PC130, Millipore, RRID:AB_2238184) for RAD51 foci detection. After washing, coverslips were incubated with Alexa 488 secondary antibodies (Thermo Fisher Scientific) and nuclei-stained with DAPI. For the CldU foci experiments, cells were previously pulsed with 10 μM CIdU for 48 hours (*53*). Images were acquired with a Leica DM4B microscope with 63× objective. At least 100 cells per condition were analyzed using the ImageJ analysis software (RRID: SCR_003070). For each nucleus, a border was created using the wand "tracing" tool on the nuclei shape in the DAPI channel. Foci within that border were counted using the "Find Maxima" function with a constant prominence value. Treatment with 0.5 mM hydroxyurea for 24 hours was used as a positive control for the CldU foci experiment.

RNA sequencing

Total RNA was extracted from cells using the TRIzol reagent (15596026, Thermo Fisher Scientific). Total RNA integrity was determined using the Agilent Bioanalyzer or 4200 TapeStation. Library preparation was performed with 5 to 10 μg of total RNA with a Bioanalyzer RNA integritty number score greater than 8.0. Ribosomal RNA was removed by poly-A selection using Oligo-dT beads (mRNA Direct kit, Life Technologies). mRNA was then fragmented in reverse transcriptase buffer and heating to 94°C for 8 min. mRNA was reverse-transcribed to yield cDNA using the SuperScript III RT enzyme (Life Technologies, per manufacturer′s instructions) and random hexamers. A second-strand reaction was performed to yield double stranded-cDNA. cDNA was blunt-ended, had an A base added to the 3′ ends, and then had Illumina sequencing adapters ligated to the ends. Ligated fragments were then amplified for 12 to 15 cycles using primers incorporating unique dual index tags. Fragments were sequenced on Illumina NovaSeq 6000 using paired end reads extending 150 bases. Basecalls and demultiplexing were performed with Illumina′s bcl2fastq2 software. RNA-seq reads were then aligned and quantitated to the Ensembl release 101 primary assembly with an Illumina DRAGEN Bio-IT server running version 3.9.3-8 software.

All gene counts were then imported into the R/Bioconductor package EdgeR, and TMM normalization size factors were calculated to adjust for samples for differences in library size (*106*). Ribosomal genes and genes not expressed in the smallest group size minus one sample greater than one count per million were excluded from further analysis. The TMM size factors and the matrix of counts were then imported into the R/Bioconductor package Limma (*106*). Weighted likelihoods based on the observed mean-variance relationship of every gene and sample were then calculated for all samples, and the count matrix was transformed to moderated $\log_2$ counts per million with Limma′s voomWithQualityWeights (*107*). Differential expression analysis was then performed to analyze for differences between conditions, and the results were filtered for only those genes with Benjamini-Hochberg false discovery rate–adjusted *P* values less than or equal to 0.05.

Quantification and statistical analysis

Statistical analysis was performed using Prism 9 (GraphPad Software, RRID: SCR_002798) and R version 4.0.2 for the ChIP-seq data. In all cases, ns indicates nonsignificant, $^{*}P \leq 0.05$, $^{**}P \leq 0.01$, $^{***}P \leq 0.001$, and $^{****}P \leq 0.0001$. Different statistical tests are applied according to the data population, and they are

indicated in the corresponding figure legends. All the experiments are performed as biological duplicates or triplicates, indicated as *N* in each figure legend.

Sequencing data analysis

The .fastq files, generated after demultiplexing of the sequencing run, were quality-controlled with FastQC (www.bioinformatics.babraham.ac.uk/projects/fastqc/) and MultiQC (*108*), trimmed with cutadapt (*109*), and aligned to hg38 reference genome with bowtie2 (*110*, *111*). Subsequently, they were sorted and indexed using Samtools (*112*) and deduplicated using the MarkDuplicates command of the Picard set of command line tools (http://broadinstitute.github.io/picard). Counts per million (CPM)–normalized BigWig files were generated using bamCoverage and bamCompare of the deepTools suite (*113*) and visualized using IGV (*114*). For determination of replication timing and early and late replicated regions, publicly available data of Repli-seq performed in RPE-1 cells generated by the Gilbert laboratory were used (*41*). The aligned .bam-files of experiment set 4DNESUNOW1OZ were downloaded from the 4DN Network (*115*, *116*) and then supplied to the Repliscan pipeline (*117*).

For determination of initiation sites, data of OK-seq in RPE-1 cells publicly available under accession number GSE114017 were used (*42*). The .fastq-files were aligned to the hg38 reference genome with bowtie2 and deduplicated using MarkDuplicates, to be in line with the ChIP-seq data. Thereafter, the R package OKseqHMM was used to determine replication initiation zones (*42*, *118*, *119*). Both the sequencing data and the package are derived from the work of Chen *et al.* (*42*). According to their publication, only replicate 1 (sample GSM3130725) was used for the determination of initiation zones.

Last, publicly available RNA-seq data in RPE-1 cells (Gene Expression Omnibus {GEO} accession number GSE146121) were used for determination of gene expression. These data were generated by Molenaar *et al.* (*120*); for this purpose, the table of read counts was downloaded from GEO, and Reads Per Kilobase Million values per gene were calculated. Last, by combining the publicly available datasets of Repli-seq, OK-seq, and RNA-seq, replication initiation sites were determined. For this purpose, TSSs of the top 50% expressed genes as measured by RNA-seq were overlapped with the initiation zones determined by OK-seq, and the early replication domain was determined by Repli-seq. The intersection of these three datasets was then used as a reference for replication initiation sites associated with transcription.

For visualization of read coverage around TSSs, early and late replicated regions as well as replication initiation sites determined via combination of publicly available data ngs.plot were used (*121*). After metagene analysis had been performed by ngs.plot, the data were replotted using the internal R plotting.

To visualize genomic tracks of early and late replicated regions and around selected initiation sites from the curated list, the UCSC genome browser, specifically the virtual machine version Genome Browser in a Box (GBIB), was used (*121*). For that purpose, CPM-normalized bedGraph files of the regions in question were generated using the bamCompare command of the deeptools suite (*113*) to consider both TOP1 ChIP-seq replicates and loaded into GBIB.

Supplementary Materials

This PDF file includes:

Figs. S1 to S7

View/request a protocol for this paper from *Bio-protocol*.

REFERENCES AND NOTES

1. J. J. Champoux, DNA topoisomerases: Structure, function, and mechanism. *Annu. Rev. Biochem.* **70**, 369–413 (2001).
2. W. Goedecke, in *xPharm: The Comprehensive Pharmacology Reference*, S. J. Enna, D. B. Bylund, Eds. (Elsevier, 2007), pp. 1–2.
3. Y. Pommier, Y. Sun, S. N. Huang, J. L. Nitiss, Roles of eukaryotic topoisomerases in transcription, replication and genomic stability. *Nat. Rev. Mol. Cell Biol.* **17**, 703–721 (2016).
4. Y. H. Hsiang, L. F. Liu, Identification of mammalian DNA topoisomerase I as an intracellular target of the anticancer drug camptothecin. *Cancer Res.* **48**, 1722–1726 (1988).
5. L. F. Liu, S. D. Desai, T. K. Li, Y. Mao, M. Sun, S. P. Sim, Mechanism of action of camptothecin. *Ann. N. Y. Acad. Sci.* **922**, 1–10 (2000).
6. V. J. Venditto, E. E. Simanek, Cancer therapies utilizing the camptothecins: A review of the in vivo literature. *Mol. Pharm.* **7**, 307–349 (2010).
7. Y. Pommier, Topoisomerase I inhibitors: Camptothecins and beyond. *Nat. Rev. Cancer* **6**, 789–802 (2006).
8. K. Shitara, Y. J. Bang, S. Iwasa, N. Sugimoto, M. H. Ryu, D. Sakai, H. C. Chung, H. Kawakami, H. Yabusaki, J. Lee, K. Saito, Y. Kawaguchi, T. Kamio, A. Kojima, M. Sugihara, K. Yamaguchi; DESTINY-Gastric01 Investigators, Trastuzumab deruxtecan in previously treated HER2-positive gastric cancer. *N. Engl. J. Med.* **382**, 2419–2430 (2020).
9. O. Yin, H. Iwata, C. C. Lin, K. Tamura, J. Watanabe, R. Wada, H. Kastrissios, M. AbuTarif, T. Garimella, C. Lee, L. Zhang, J. Shahidi, F. LaCreta, Exposure-response relationships in patients with HER2-positive metastatic breast cancer and other solid tumors treated with trastuzumab deruxtecan. *Clin. Pharmacol. Ther.* **110**, 986–996 (2021).
10. S. Modi, C. Saura, T. Yamashita, Y. H. Park, S. B. Kim, K. Tamura, F. Andre, H. Iwata, Y. Ito, J. Tsurutani, J. Sohn, N. Denduluri, C. Perrin, K. Aogi, E. Tokunaga, S. A. Im, K. S. Lee, S. A. Hurvitz, J. Cortes, C. Lee, S. Chen, L. Zhang, J. Shahidi, A. Yver, I. Krop; DESTINY-Breast01 Investigators, Trastuzumab deruxtecan in previously treated HER2-positive breast cancer. *N. Engl. J. Med.* **382**, 610–621 (2020).
11. G. L. Beretta, L. Gatti, P. Perego, N. Zaffaroni, Camptothecin resistance in cancer: Insights into the molecular mechanisms of a DNA-damaging drug. *Curr. Med. Chem.* **20**, 1541–1565 (2013).
12. M. Berti, A. Ray Chaudhuri, S. Thangavel, S. Gomathinayagam, S. Kenig, M. Vujanovic, F. Odreman, T. Glatter, S. Graziano, R. Mendoza-Maldonado, F. Marino, B. Lucic, V. Biasin, M. Gstaiger, R. Aebersold, J. M. Sidorova, R. J. Monnat Jr., M. Lopes, A. Vindigni, Human RECQ1 promotes restart of replication forks reversed by DNA topoisomerase I inhibition. *Nat. Struct. Mol. Biol.* **20**, 347–354 (2013).
13. A. Ray Chaudhuri, Y. Hashimoto, R. Herrador, K. J. Neelsen, D. Fachinetti, R. Bermejo, A. Cocito, V. Costanzo, M. Lopes, Topoisomerase I poisoning results in PARP-mediated replication fork reversal. *Nat. Struct. Mol. Biol.* **19**, 417–423 (2012).
14. D. Strumberg, A. A. Pilon, M. Smith, R. Hickey, L. Malkas, Y. Pommier, Conversion of topoisomerase I cleavage complexes on the leading strand of ribosomal DNA into 5′-phosphorylated DNA double-strand breaks by replication runoff. *Mol. Cell. Biol.* **20**, 3977–3987 (2000).
15. Y. Pommier, C. Redon, V. A. Rao, J. A. Seiler, O. Sordet, H. Takemura, S. Antony, L. Meng, Z. Liao, G. Kohlhagen, H. Zhang, K. W. Kohn, Repair of and checkpoint response to topoisomerase I-mediated DNA damage. *Mutat. Res.* **532**, 173–203 (2003).
16. C. Holm, J. M. Covey, D. Kerrigan, Y. Pommier, Differential requirement of DNA replication for the cytotoxicity of DNA topoisomerase I and II inhibitors in Chinese hamster DC3F cells. *Cancer Res.* **49**, 6365–6368 (1989).
17. Y. H. Hsiang, M. G. Lihou, L. F. Liu, Arrest of replication forks by drug-stabilized topoisomerase I-DNA cleavable complexes as a mechanism of cell killing by camptothecin. *Cancer Res.* **49**, 5077–5082 (1989).
18. Y. H. Hsiang, L. F. Liu, M. E. Wall, M. C. Wani, A. W. Nicholas, G. Manikumar, S. Kirschenbaum, R. Silber, M. Potmesil, DNA topoisomerase I-mediated DNA cleavage and cytotoxicity of camptothecin analogues. *Cancer Res.* **49**, 4385–4389 (1989).
19. Y. Sun, L. K. Saha, S. Saha, U. Jo, Y. Pommier, Debulking of topoisomerase DNA-protein crosslinks (TOP-DPC) by the proteasome, non-proteasomal and non-proteolytic pathways. *DNA Repair* **94**, 102926 (2020).
20. I. Plo, Z. Y. Liao, J. M. Barceló, G. Kohlhagen, K. W. Caldecott, M. Weinfeld, Y. Pommier, Association of XRCC1 and tyrosyl DNA phosphodiesterase (Tdp1) for the repair of topoisomerase I-mediated DNA lesions. *DNA Repair* **2**, 1087–1100 (2003).

21. Y. Pommier, S. Y. N. Huang, R. Gao, B. B. das, J. Murai, C. Marchand, Tyrosyl-DNA-phosphodiesterases (TDP1 and TDP2). *DNA Repair* **19**, 114–129 (2014).
22. H. Interthal, H. J. Chen, T. E. Kehl-Fie, J. Zotzmann, J. B. Leppard, J. J. Champoux, SCAN1 mutant Tdp1 accumulates the enzyme--DNA intermediate and causes camptothecin hypersensitivity. *EMBO J.* **24**, 2224–2233 (2005).
23. S. F. El-Khamisy, G. M. Saifi, M. Weinfeld, F. Johansson, T. Helleday, J. R. Lupski, K. W. Caldecott, Defective DNA single-strand break repair in spinocerebellar ataxia with axonal neuropathy-1. *Nature* **434**, 108–113 (2005).
24. S. D. Desai, L. F. Liu, D. Vazquez-Abad, P. D'Arpa, Ubiquitin-dependent destruction of topoisomerase I is stimulated by the antitumor drug camptothecin. *J. Biol. Chem.* **272**, 24159–24164 (1997).
25. H. F. Zhang, A. Tomida, R. Koshimizu, Y. Ogiso, S. Lei, T. Tsuruo, Cullin 3 promotes proteasomal degradation of the topoisomerase I-DNA covalent complex. *Cancer Res.* **64**, 1114–1121 (2004).
26. C. Kerzendorfer, A. Whibley, G. Carpenter, E. Outwin, S. C. Chiang, G. Turner, C. Schwartz, S. el-Khamisy, F. L. Raymond, M. O'Driscoll, Mutations in Cullin 4B result in a human syndrome associated with increased camptothecin-induced topoisomerase I-dependent DNA breaks. *Hum. Mol. Genet.* **19**, 1324–1334 (2010).
27. O. Sordet, S. Larochelle, E. Nicolas, E. V. Stevens, C. Zhang, K. M. Shokat, R. P. Fisher, Y. Pommier, Hyperphosphorylation of RNA polymerase II in response to topoisomerase I cleavage complexes and its association with transcription- and BRCA1-dependent degradation of topoisomerase I. *J. Mol. Biol.* **381**, 540–549 (2008).
28. V. Menon, L. F. Povirk, End-processing nucleases and phosphodiesterases: An elite supporting cast for the non-homologous end joining pathway of DNA double-strand break repair. *DNA Repair* **43**, 57–68 (2016).
29. Y. Sun, S. Saha, W. Wang, L. K. Saha, S.-Y. N. Huang, Y. Pommier, Excision repair of topoisomerase DNA-protein crosslinks (TOP-DPC). *DNA Repair* **89**, 102837 (2020).
30. R. S. Maskey, K. S. Flatten, C. J. Sieben, K. L. Peterson, D. J. Baker, H.-J. Nam, M. S. Kim, T. C. Smyrk, Y. Kojima, Y. Machida, A. Santiago, J. M. van Deursen, S. H. Kaufmann, Y. J. Machida, Spartan deficiency causes accumulation of Topoisomerase 1 cleavage complexes and tumorigenesis. *Nucleic Acids Res.* **45**, 4564–4576 (2017).
31. J. Stingele, M. S. Schwarz, N. Bloemeke, P. G. Wolf, S. Jentsch, A DNA-dependent protease involved in DNA-protein crosslink repair. *Cell* **158**, 327–338 (2014).
32. L. K. Lerner, G. Francisco, D. T. Soltys, C. R. R. Rocha, A. Quinet, A. T. Vessoni, L. P. Castro, T. I. P. David, S. O. Bustos, B. E. Strauss, V. Gottifredi, A. Stary, A. Sarasin, R. Chammas, C. F. M. Menck, Predominant role of DNA polymerase eta and p53-dependent translesion synthesis in the survival of ultraviolet-irradiated human cells. *Nucleic Acids Res.* **45**, 1270–1280 (2017).
33. W. M. Bonner, Low-dose radiation: Thresholds, bystander effects, and adaptive responses. *Proc. Natl. Acad. Sci. U.S.A.* **100**, 4973–4975 (2003).
34. D. R. Crawford, K. J. Davies, Adaptive response and oxidative stress. *Environ. Health Perspect.* **102** (Suppl. 10), 25–28 (1994).
35. Y. Gueguen, A. Bontemps, T. G. Ebrahimian, Adaptive responses to low doses of radiation or chemicals: Their cellular and molecular mechanisms. *Cell. Mol. Life Sci.* **76**, 1255–1273 (2019).
36. J. D. Shadley, J. K. Wiencke, Induction of the adaptive response by X-rays is dependent on radiation intensity. *Int. J. Radiat. Biol.* **56**, 107–118 (1989).
37. G. Olivieri, J. Bodycote, S. Wolff, Adaptive response of human lymphocytes to low concentrations of radioactive thymidine. *Science* **223**, 594–597 (1984).
38. A. Quinet, S. Tirman, J. Jackson, S. Šviković, D. Lemaçon, D. Carvajal-Maldonado, D. González-Acosta, A. T. Vessoni, E. Cybulla, M. Wood, S. Tavis, L. F. Z. Batista, J. Méndez, J. E. Sale, A. Vindigni, PRIMPOL-mediated adaptive response suppresses replication fork reversal in BRCA-deficient cells. *Mol. Cell* **77**, 461–474.e9 (2020).
39. L. Baranello, D. Wojtowicz, K. Cui, B. N. Devaiah, H.-J. Chung, K. Y. Chan-Salis, R. Guha, K. Wilson, X. Zhang, H. Zhang, J. Piotrowski, C. J. Thomas, D. S. Singer, B. F. Pugh, Y. Pommier, T. M. Przytycka, F. Kouzine, B. A. Lewis, K. Zhao, D. Levens, RNA polymerase II regulates topoisomerase 1 activity to favor efficient transcription. *Cell* **165**, 357–371 (2016).
40. J. E. Deweese, M. A. Osheroff, N. Osheroff, DNA topology and topoisomerases: Teaching a "Knotty" subject. *Biochem. Mol. Biol. Educ.* **37**, 2–10 (2008).
41. C. Marchal, T. Sasaki, D. Vera, K. Wilson, J. Sima, J. C. Rivera-Mulia, C. Trevilla-García, C. Nogues, E. Nafie, D. M. Gilbert, Genome-wide analysis of replication timing by next-generation sequencing with E/L Repli-seq. *Nat. Protoc.* **13**, 819–839 (2018).
42. Y.-H. Chen, S. Keegan, M. Kahli, P. Tonzi, D. Fenyö, T. T. Huang, D. J. Smith, Transcription shapes DNA replication initiation and termination in human cells. *Nat. Struct. Mol. Biol.* **26**, 67–77 (2019).
43. Y. Liu, C. Ai, T. Gan, J. Wu, Y. Jiang, X. Liu, R. Lu, N. Gao, Q. Li, X. Ji, J. Hu, Transcription shapes DNA replication initiation to preserve genome integrity. *Genome Biol.* **22**, 176 (2021).
44. G. Abdurashidova, S. Radulescu, O. Sandoval, S. Zahariev, M. B. Danailov, A. Demidovich, L. Santamaria, G. Biamonti, S. Riva, A. Falaschi, Functional interactions of DNA topoisomerases with a human replication origin. *EMBO J.* **26**, 998–1009 (2007).
45. A. Kegel, H. Betts-Lindroos, T. Kanno, K. Jeppsson, L. Ström, Y. Katou, T. Itoh, K. Shirahige, C. Sjögren, Chromosome length influences replication-induced topological stress. *Nature* **471**, 392–396 (2011).
46. S. K. L. Lui, S. Keegan, P. Tonzi, M. Kahli, Y.-H. Chen, N. Chalhoub, K. E. Coleman, D. Fenyo, D. J. Smith, T. T. Huang, Monitoring genome-wide replication fork directionality by Okazaki fragment sequencing in mammalian cells. *Nat. Protoc.* **16**, 1193–1218 (2021).
47. K. Kiianitsa, N. Maizels, A rapid and sensitive assay for DNA-protein covalent complexes in living cells. *Nucleic Acids Res.* **41**, e104 (2013).
48. A. Meroni, A. Vindigni, A RADAR method to measure DNA topoisomerase covalent complexes, in *Methods in Enzymology*, M. A. Trakselis, Ed. (Academic Press Inc., 2022).
49. C. Gongora, N. Vezzio-Vie, S. Tuduri, V. Denis, A. Causse, C. Auzanneau, G. Collod-Beroud, A. Coquelle, P. Pasero, P. Pourquier, P. Martineau, M. D. Rio, New Topoisomerase I mutations are associated with resistance to camptothecin. *Mol. Cancer* **10**, 1–13 (2011).
50. G. Bai, C. Kermi, H. Stoy, C. J. Schiltz, J. Bacal, A. M. Zaino, M. K. Hadden, B. F. Eichman, M. Lopes, K. A. Cimprich, HLTF promotes fork reversal, limiting replication stress resistance and preventing multiple mechanisms of unrestrained DNA synthesis. *Mol. Cell* **78**, 1237–1251.e7 (2020).
51. M.-M. Genois, J.-P. Gagné, T. Yasuhara, J. Jackson, S. Saxena, M.-F. Langelier, I. Ahel, M. T. Bedford, J. M. Pascal, A. Vindigni, G. G. Poirier, L. Zou, CARM1 regulates replication fork speed and stress response by stimulating PARP1. *Mol. Cell* **81**, 784–800.e8 (2021).
52. A. Quinet, D. Carvajal-Maldonado, D. Lemacon, A. Vindigni, DNA fiber analysis: Mind the Gap! *Methods Enzymol.* **591**, 55–82 (2017).
53. K. Cong, M. Peng, A. N. Kousholt, W. T. C. Lee, S. Lee, S. Nayak, J. Krais, P. S. Vander VereCarozza, K. S. Pawelczak, J. Calvo, N. J. Panzarino, J. J. Turchi, N. Johnson, J. Jonkers, E. Rothenberg, S. B. Cantor, Replication gaps are a key determinant of PARP inhibitor synthetic lethality with BRCA deficiency. *Mol. Cell* **81**, 3128–3144.e7 (2021).
54. K. Watanabe, S. Tateishi, M. Kawasuji, T. Tsurimoto, H. Inoue, M. Yamaizumi, Rad18 guides poleta to replication stalling sites through physical interaction and PCNA monoubiquitination. *EMBO J.* **23**, 3886–3896 (2004).
55. S. D. Desai, T. K. Li, A. Rodriguez-Bauman, E. H. Rubin, L. F. Liu, Ubiquitin/26S proteasome-mediated degradation of topoisomerase I as a resistance mechanism to camptothecin in tumor cells. *Cancer Res.* **61**, 5926–5932 (2001).
56. C. P. Lin, Y. Ban, Y. L. Lyu, S. D. Desai, L. F. Liu, A ubiquitin-proteasome pathway for the repair of topoisomerase I-DNA covalent complexes. *J. Biol. Chem.* **283**, 21074–21083 (2008).
57. M. L. Hyer, M. A. Milhollen, J. Ciavarri, P. Fleming, T. Traore, D. Sappal, J. Huck, J. Shi, J. Gavin, J. Brownell, Y. Yang, B. Stringer, R. Griffin, F. Bruzzese, T. Soucy, J. Duffy, C. Rabino, J. Riceberg, K. Hoar, A. Lublinsky, S. Menon, M. Sintchak, N. Bump, S. M. Pulukuri, S. Langston, S. Tirrell, M. Kuranda, P. Veiby, J. Newcomb, P. Li, J. T. Wu, J. Powe, L. R. Dick, P. Greenspan, K. Galvin, M. Manfredi, C. Claiborne, B. S. Amidon, N. F. Bence, A small-molecule inhibitor of the ubiquitin activating enzyme for cancer treatment. *Nat. Med.* **24**, 186–193 (2018).
58. Y. Murai, U. Jo, J. Murai, L. M. Jenkins, S.-Y. N. Huang, S. Chakka, L. Chen, K. Cheng, S. Fukuda, N. Takebe, Y. Pommier, SLFN11 inactivation induces proteotoxic stress and sensitizes cancer cells to ubiquitin activating enzyme inhibitor TAK-243. *Cancer Res.* **81**, 3067–3078 (2021).
59. Y. Sun, L. M. Miller Jenkins, Y. P. Su, K. C. Nitiss, J. L. Nitiss, Y. Pommier, A conserved SUMO pathway repairs topoisomerase DNA-protein cross-links by engaging ubiquitin-mediated proteasomal degradation. *Sci. Adv.* **6**, eaba6290 (2020).
60. L. Xu, L. Yang, K. Hashimoto, M. Anderson, G. Kohlhagen, Y. Pommier, P. D'Arpa, Characterization of BTBD1 and BTBD2, two similar BTB-domain-containing Kelch-like proteins that interact with Topoisomerase I. *BMC Genomics* **3**, 1 (2002).
61. G. Rabut, M. Peter, Function and regulation of protein neddylation.'Protein modifications: Beyond the usual suspects' review series. *EMBO Rep.* **9**, 969–976 (2008).
62. J. S. Brown, S. P. Jackson, Ubiquitylation, neddylation and the DNA damage response. *Open Biol.* **5**, 150018 (2015).
63. L. Zhou, W. Zhang, Y. Sun, L. Jia, Protein neddylation and its alterations in human cancers for targeted therapy. *Cell. Signal.* **44**, 92–102 (2018).
64. M. Ohh, W. Y. Kim, J. J. Moslehi, Y. Chen, V. Chau, M. A. Read, W. G. Kaelin Jr., An intact NEDD8 pathway is required for Cullin-dependent ubiquitylation in mammalian cells. *EMBO Rep.* **3**, 177–182 (2002).
65. F. Osaka, M. Saeki, S. Katayama, N. Aida, A. Toh-E, K. Kominami, T. Toda, T. Suzuki, T. Chiba, K. Tanaka, S. Kato, Covalent modifier NEDD8 is essential for SCF ubiquitin-ligase in fission yeast. *EMBO J.* **19**, 3475–3484 (2000).

66. L. Pintard, T. Kurz, S. Glaser, J. H. Willis, M. Peter, B. Bowerman, Neddylation and deneddylation of CUL-3 is required to target MEI-1/Katanin for degradation at the meiosis-to-mitosis transition in C. elegans. *Curr. Biol.* **13**, 911–921 (2003).
67. J. E. Brownell, M. D. Sintchak, J. M. Gavin, H. Liao, F. J. Bruzzese, N. J. Bump, T. A. Soucy, M. A. Milhollen, X. Yang, A. L. Burkhardt, J. Ma, H.-K. Loke, T. Lingaraj, D. Wu, K. B. Hamman, J. J. Spelman, C. A. Cullis, S. P. Langston, S. Vyskocil, T. B. Sells, W. D. Mallender, I. Visiers, P. Li, C. F. Claiborne, M. Rolfe, J. B. Bolen, L. R. Dick, Substrate-assisted inhibition of ubiquitin-like protein-activating enzymes: The NEDD8 E1 inhibitor MLN4924 forms a NEDD8-AMP mimetic in situ. *Mol. Cell* **37**, 102–111 (2010).
68. T. A. Soucy, P. G. Smith, M. A. Milhollen, A. J. Berger, J. M. Gavin, S. Adhikari, J. E. Brownell, K. E. Burke, D. P. Cardin, S. Critchley, C. A. Cullis, A. Doucette, J. J. Garnsey, J. L. Gaulin, R. E. Gershman, A. R. Lublinsky, A. M. Donald, H. Mizutani, U. Narayanan, E. J. Olhava, S. Peluso, M. Rezaei, M. D. Sintchak, T. Talreja, M. P. Thomas, T. Traore, S. Vyskocil, G. S. Weatherhead, J. Yu, J. Zhang, L. R. Dick, C. F. Claiborne, M. Rolfe, J. B. Bolen, S. P. Langston, An inhibitor of NEDD8-activating enzyme as a new approach to treat cancer. *Nature* **458**, 732–736 (2009).
69. W. Wimuttisuk, J. D. Singer, The Cullin3 ubiquitin ligase functions as a Nedd8-bound heterodimer. *Mol. Biol. Cell* **18**, 899–909 (2007).
70. J. R. Lydeard, B. A. Schulman, J. W. Harper, Building and remodelling Cullin-RING E3 ubiquitin ligases. *EMBO Rep.* **14**, 1050–1061 (2013).
71. T. A. Soucy, L. R. Dick, P. G. Smith, M. A. Milhollen, J. E. Brownell, The NEDD8 conjugation pathway and its relevance in cancer biology and therapy. *Genes Cancer* **1**, 708–716 (2010).
72. V. Pavillard, C. Agostini, S. Richard, V. Charasson, D. Montaudon, J. Robert, Determinants of the cytotoxicity of irinotecan in two human colorectal tumor cell lines. *Cancer Chemother. Pharmacol.* **49**, 329–335 (2002).
73. G. Caceres, R. Zankina, X. Y. Zhu, J. Jiao, H. Wong, A. Aller, P. Andreotti, Determination of chemotherapeutic activity in vivo by luminescent imaging of luciferase-transfected human tumors. *Anticancer Drugs* **14**, 569–574 (2003).
74. C. F. Stewart, L. C. Iacono, M. Chintagumpala, S. J. Kellie, D. Ashley, W. C. Zamboni, M. N. Kirstein, M. Fouladi, L. G. Seele, D. Wallace, P. J. Houghton, A. Gajjar, Results of a phase II upfront window of pharmacokinetically guided topotecan in high-risk medulloblastoma and supratentorial primitive neuroectodermal tumor. *J. Clin. Oncol.* **22**, 3357–3365 (2004).
75. C. M. F. Kruijtzer, J. H. Beijnen, H. Rosing, W. W. ten Bokkel Huinink, M. Schot, R. C. Jewell, E. M. Paul, J. H. M. Schellens, Increased oral bioavailability of topotecan in combination with the breast cancer resistance protein and P-glycoprotein inhibitor GF120918. *J. Clin. Oncol.* **20**, 2943–2950 (2002).
76. G. G. Chabot, Clinical pharmacokinetics of irinotecan. *Clin. Pharmacokinet.* **33**, 245–259 (1997).
77. A. Sparreboom, D. F. S. Kehrer, R. H. J. Mathijssen, R. Xie, M. J. A. de Jonge, P. de Bruijn, A. S. T. Planting, F. A. L. M. Eskens, C. Verheij, G. de Heus, A. Klaren, S. Zhang, T. Verhaeghe, P. A. Palmer, J. Verweij, Phase I and pharmacokinetic study of irinotecan in combination with R115777, a farnesyl protein transferase inhibitor. *Br. J. Cancer* **90**, 1508–1515 (2004).
78. C. Fuchs, E. P. Mitchell, P. M. Hoff, Irinotecan in the treatment of colorectal cancer. *Cancer Treat. Rev.* **32**, 491–503 (2006).
79. K. Fujita, Y. Kubota, H. Ishida, Y. Sasaki, Irinotecan, a key chemotherapeutic drug for metastatic colorectal cancer. *World J. Gastroenterol.* **21**, 12234–12248 (2015).
80. L. M. Wagner, Fifteen years of irinotecan therapy for pediatric sarcoma: Where to next? *Clin. Sarcoma Res.* **5**, 20 (2015).
81. T. Higuchi, K. Miyake, H. Oshiro, N. Sugisawa, N. Yamamoto, K. Hayashi, H. Kimura, S. Miwa, K. Igarashi, S. P. Chawla, M. Bouvet, S. R. Singh, H. Tsuchiya, R. M. Hoffman, Trabectedin and irinotecan combination regresses a cisplatinum-resistant osteosarcoma in a patient-derived orthotopic xenograft nude-mouse model. *Biochem. Biophys. Res. Commun.* **513**, 326–331 (2019).
82. A. R. Sarasin, P. C. Hanawalt, Carcinogens enhance survival of UV-irradiated simian virus 40 in treated monkey kidney cells: Induction of a recovery pathway? *Proc. Natl. Acad. Sci. U.S.A.* **75**, 346–350 (1978).
83. S. Tuduri, L. Crabbé, C. Conti, H. Tourrière, H. Holtgreve-Grez, A. Jauch, V. Pantesco, J. De Vos, A. Thomas, C. Theillet, Y. Pommier, J. Tazi, A. Coquelle, P. Pasero, Topoisomerase I suppresses genomic instability by preventing interference between replication and transcription. *Nat. Cell Biol.* **11**, 1315–1324 (2009).
84. S. G. Manzo, S. R. Hartono, L. A. Sanz, J. Marinello, S. De Biasi, A. Cossarizza, G. Capranico, F. Chedin, DNA Topoisomerase I differentially modulates R-loops across the human genome. *Genome Biol.* **19**, 100 (2018).
85. S. K. Das, V. Kuzin, D. P. Cameron, S. Sanford, R. K. Jha, Z. Nie, M. T. Rosello, R. Holewinski, T. Andresson, J. Wisniewski, T. Natsume, D. H. Price, B. A. Lewis, F. Kouzine, D. Levens, L. Baranello, MYC assembles and stimulates topoisomerases 1 and 2 in a "topoisome". *Mol. Cell* **82**, 140–158.e12 (2022).
86. A. Wiegard, V. Kuzin, D. P. Cameron, J. Grosser, M. Ceribelli, R. Mehmood, R. Ballarino, F. Valant, R. Grochowski, I. Karabogdan, N. Crosetto, A. Lindqvist, A. H. Bizard, F. Kouzine, T. Natsume, L. Baranello, Topoisomerase 1 activity during mitotic transcription favors the transition from mitosis to G1. *Mol. Cell* **81**, 5007–5024.e9 (2021).
87. K. Mutreja, J. Krietsch, J. Hess, S. Ursich, M. Berti, F. K. Roessler, R. Zellweger, M. Patra, G. Gasser, M. Lopes, ATR-mediated global fork slowing and reversal assist fork traverse and prevent chromosomal breakage at DNA interstrand cross-links. *Cell Rep.* **24**, 2629–2642.e5 (2018).
88. E. J. Sacho, N. Maizels, DNA repair factor MRE11/RAD50 cleaves 3′-phosphotyrosyl bonds and resects DNA to repair damage caused by topoisomerase 1 poisons. *J. Biol. Chem.* **286**, 44945–44951 (2011).
89. E. Hartsuiker, M. J. Neale, A. M. Carr, Distinct requirements for the Rad32(Mre11) nuclease and Ctp1(CtIP) in the removal of covalently bound topoisomerase I and II from DNA. *Mol. Cell* **33**, 117–123 (2009).
90. C. Takahata, Y. Masuda, A. Takedachi, K. Tanaka, S. Iwai, I. Kuraoka, Repair synthesis step involving ERCC1-XPF participates in DNA repair of the Top1-DNA damage complex. *Carcinogenesis* **36**, 841–851 (2015).
91. C. Liu, J. J. Pouliot, H. A. Nash, Repair of topoisomerase I covalent complexes in the absence of the tyrosyl-DNA phosphodiesterase Tdp1. *Proc. Natl. Acad. Sci. U.S.A.* **99**, 14970–14975 (2002).
92. Y. Kim, G. S. Spitz, U. Veturi, F. P. Lach, A. D. Auerbach, A. Smogorzewska, Regulation of multiple DNA repair pathways by the Fanconi anemia protein SLX4. *Blood* **121**, 54–63 (2013).
93. M. D. Petroski, R. J. Deshaies, Function and regulation of cullin-RING ubiquitin ligases. *Nat. Rev. Mol. Cell Biol.* **6**, 9–20 (2005).
94. C. Ribeyre, R. Zellweger, M. Chauvin, N. Bec, C. Larroque, M. Lopes, A. Constantinou, Nascent DNA proteomics reveals a chromatin remodeler required for topoisomerase I loading at replication forks. *Cell Rep.* **15**, 300–309 (2016).
95. J. Lopez-Mosqueda, K. Maddi, S. Prgomet, S. Kalayil, I. Marinovic-Terzic, J. Terzic, I. Dikic, SPRTN is a mammalian DNA-binding metalloprotease that resolves DNA-protein crosslinks. *eLife* **5**, (2016).
96. M. Mórocz, E. Zsigmond, R. Tóth, M. Z. Enyedi, L. Pintér, L. Haracska, DNA-dependent protease activity of human Spartan facilitates replication of DNA-protein crosslink-containing DNA. *Nucleic Acids Res.* **45**, 3172–3188 (2017).
97. Y. Kojima, Y. Machida, S. Palani, T. R. Caulfield, E. S. Radisky, S. H. Kaufmann, Y. J. Machida, FAM111A protects replication forks from protein obstacles via its trypsin-like domain. *Nat. Commun.* **11**, 1318 (2020).
98. A. Craig Lockhart, T. M. Bauer, C. Aggarwal, C. B. Lee, R. D. Harvey, R. B. Cohen, F. Sedarati, T. K. Nip, H. Faessel, A. B. Dash, B. J. Dezube, D. V. Faller, A. Dowlati, Phase Ib study of pevonedistat, a NEDD8-activating enzyme inhibitor, in combination with docetaxel, carboplatin and paclitaxel, or gemcitabine, in patients with advanced solid tumors. *Invest. New Drugs* **37**, 87–97 (2019).
99. X. Zhou, S. Friedlander, E. Kupperman, F. Sedarati, S. Kuroda, Z. Hua, Y. Yuan, Y. Yamamoto, D. V. Faller, K. Haikawa, K. Nakai, S. Bowen, Y. Dai, K. Venkatakrishnan, Asia-inclusive global development of pevonedistat: Clinical pharmacology and translational research enabling a phase 3 multiregional clinical trial. *Clin. Transl. Sci.* **14**, 1069–1081 (2021).
100. X. Zhou, F. Sedarati, D. V. Faller, D. Zhao, H. M. Faessel, S. Chowdhury, J. Bolleddula, Y. Li, K. Venkatakrishnan, Z. Papai, Phase I study assessing the mass balance, pharmacokinetics, and excretion of [14C]-pevonedistat, a NEDD8-activating enzyme inhibitor in patients with advanced solid tumors. *Invest. New Drugs* **39**, 488–498 (2021).
101. D. P. Cameron, V. Kuzin, L. Baranello, Analysis of myc chromatin binding by calibrated ChIP-Seq approach. *Methods Mol. Biol.* **2318**, 161–185 (2021).
102. J.-H. Yoon, S. Prakash, L. Prakash, Requirement of Rad18 protein for replication through DNA lesions in mouse and human cells. *Proc. Natl. Acad. Sci. U.S.A.* **109**, 7799–7804 (2012).
103. C. P. García, G. A. V. Richardson, L. Romorini, S. G. Miriuka, G. E. Sevlever, M. E. Scassa, Topoisomerase I inhibitor, camptothecin, induces apoptogenic signaling in human embryonic stem cells. *Stem Cell Res.* **12**, 400–414 (2014).
104. A. Meroni, G. M. Nava, E. Bianco, L. Grasso, E. Galati, M. C. Bosio, D. Delmastro, M. Muzi-Falconi, F. Lazzaro, RNase H activities counteract a toxic effect of Polymerase η in cells replicating with depleted dNTP pools. *Nucleic Acids Res.* **47**, 4612–4623 (2019).
105. S. Tirman, A. Quinet, M. Wood, A. Meroni, E. Cybulla, J. Jackson, S. Pegoraro, A. Simoneau, L. Zou, A. Vindigni, Temporally distinct post-replicative repair mechanisms fill PRIMPOL-dependent ssDNA gaps in human cells. *Mol. Cell* **81**, 4026–4040.e8 (2021).
106. M. E. Ritchie, B. Phipson, D. Wu, Y. Hu, C. W. Law, W. Shi, G. K. Smyth, limma powers differential expression analyses for RNA-sequencing and microarray studies. *Nucleic Acids Res.* **43**, e47 (2015).
107. R. Liu, A. Z. Holik, S. Su, N. Jansz, K. Chen, H. S. Leong, M. E. Blewitt, M.-L. Asselin-Labat, G. K. Smyth, M. E. Ritchie, Why weight? Modelling sample and observational level variability improves power in RNA-seq analyses. *Nucleic Acids Res.* **43**, e97 (2015).

108. P. Ewels, M. Magnusson, S. Lundin, M. Käller, MultiQC: Summarize analysis results for multiple tools and samples in a single report. *Bioinformatics* **32**, 3047–3048 (2016).
109. M. Martin, Cutadapt removes adapter sequences from high-throughput sequencing reads. *EMBnet J.* **17**, 3 (2011).
110. B. Langmead, S. L. Salzberg, Fast gapped-read alignment with Bowtie 2. *Nat. Methods* **9**, 357–359 (2012).
111. B. Langmead, C. Wilks, V. Antonescu, R. Charles, Scaling read aligners to hundreds of threads on general-purpose processors. *Bioinformatics* **35**, 421–432 (2019).
112. H. Li, B. Handsaker, A. Wysoker, T. Fennell, J. Ruan, N. Homer, G. Marth, G. Abecasis, R. Durbin, The sequence alignment/map format and SAMtools. *Bioinformatics* **25**, 2078–2079 (2009).
113. F. Ramírez, D. P. Ryan, B. Grüning, V. Bhardwaj, F. Kilpert, A. S. Richter, S. Heyne, F. Dündar, T. Manke, deepTools2: A next generation web server for deep-sequencing data analysis. *Nucleic Acids Res.* **44**, W160–W165 (2016).
114. J. T. Robinson, H. Thorvaldsdóttir, W. Winckler, M. Guttman, E. S. Lander, G. Getz, J. P. Mesirov, Integrative genomics viewer. *Nat. Biotechnol.* **29**, 24–26 (2011).
115. J. Dekker, A. S. Belmont, M. Guttman, V. O. Leshyk, J. T. Lis, S. Lomvardas, L. A. Mirny, C. C. O'Shea, P. J. Park, B. Ren, J. C. R. Politz, J. Shendure, S. Zhong; 4D Nucleome Network, The 4D nucleome project. *Nature* **549**, 219–226 (2017).
116. S. B. Reiff, A. J. Schroeder, K. Kırlı, A. Cosolo, C. Bakker, L. Mercado, S. Lee, A. D. Veit, A. K. Balashov, C. Vitzthum, W. Ronchetti, K. M. Pitman, J. Johnson, S. R. Ehmsen, P. Kerpedjiev, N. Abdennur, M. Imakaev, S. U. Öztürk, U. Çamoğlu, L. A. Mirny, N. Gehlenborg, B. H. Alver, P. J. Park, The 4D nucleome data portal as a resource for searching and visualizing curated nucleomics data. *Nat. Commun.* **13**, 2365 (2022).
117. G. J. Zynda, J. Song, L. Concia, E. E. Wear, L. Hanley-Bowdoin, W. F. Thompson, M. W. Vaughn, Repliscan: A tool for classifying replication timing regions. *BMC Bioinformatics* **18**, 362 (2017).
118. Y. Liu, X. Wu, Y. D'aubenton-Carafa, C. Thermes, C.-L. Chen, OKseqHMM: A genome-wide replication fork directionality analysis toolkit. bioRxiv 2022.01.12.476022 [**Preprint**]. 13 January 2022. https://doi.org/10.1101/2022.01.12.476022.
119. A. Promonet, I. Padioleau, Y. Liu, L. Sanz, A. Biernacka, A.-L. Schmitz, M. Skrzypczak, A. Sarrazin, C. Mettling, M. Rowicka, K. Ginalski, F. Chedin, C.-L. Chen, Y.-L. Lin, P. Pasero, Topoisomerase 1 prevents replication stress at R-loop-enriched transcription termination sites. *Nat. Commun.* **11**, 3940 (2020).
120. T. M. Molenaar, M. Pagès-Gallego, V. Meyn, F. van Leeuwen, Application of recombination-induced tag exchange (RITE) to study histone dynamics in human cells. *Epigenetics* **15**, 901–913 (2020).
121. L. Shen, N. Shao, X. Liu, E. Nestler, ngs.plot: Quick mining and visualization of next-generation sequencing data by integrating genomic databases. *BMC Genomics* **15**, 284 (2014).

Acknowledgments: We would like to thank K. Caldecott (University of Sussex, UK) for providing the TDP1 KO RPE1 cells, S. El-Khamisy (University of Sheffield, UK) for providing the colon cancer cells (RKO), and S. Devarakonda (Washington University, St. Louis, MO, USA) for the useful discussions about the clinical relevance of our findings. We thank C. Kutter and K. Geng for technical expertise with sequencing. Figures were created with BioRender.com. **Funding:** This work was supported by National Cancer Institute grants R01CA237263 and R01CA248526 (A.V.), U.S. Department of Defense (DOD) Breast Cancer Research Program (BRCP) Expansion Award BC191374 (A.V.), The Alvin J. Siteman Cancer Center Siteman Investment Program (supported by The Foundation for Barnes-Jewish Hospital, Cancer Frontier Fund) (A.V.), The Barnard Foundation (A.V.), a fellowship from the American Italian Cancer Foundation (A.M.), The Wallenberg Foundation grant KAW 2016.0161 (L.B.), The Swedish Research Council grant 2016-02610 VR (L.B.), The Cancerfonden grant 21 1771 Pj 01 (L.B.), The Cancerfonden grant CAN 2018/760 (L.B.), and The Karolinska Institutet KID grant 2018 (L.B.) **Author contributions:** A.M. carried out all the cellular and biochemical experiments. J.G. performed the ChIP-seq experiments and analyzed all the sequencing data. S.A. contributed with some of the DNA fiber experiments. N.R. performed the immunofluorescence experiments to monitor ssDNA accumulation. J.J. contributed to some of the biochemical experiments. L.B. supervised and designed all the sequencing experiments with J.G. A.M. and A.V. designed the project. A.V. supervised the project and wrote the manuscript with A.M., with input from all other authors. **Competing interests:** The authors declare that they have no competing interests. **Data and materials availability:** All data needed to evaluate the conclusions in the paper are present in the paper and/or the Supplementary Materials. ChIP-seq and RNA-seq data reported in this paper were deposited as series GSE212470 (ChIP-seq: GSE212468; RNA-seq: GSE212469) in the GEO database (https://www.ncbi.nlm.nih.gov/geo/) and are publicly available as of the date of publication. Previously published sequencing data [Repli-seq: 4DN Network (https://data.4dnucleome.org/), experiment set 4DNESUNOW1OZ; OK-seq: GEO, GSE114017; and RNA-seq: GEO, GSE146121] are available from the respective repositories as indicated. Further information and requests for resources and reagents should be directed to A.V. (avindigni@wustl.edu). The original datasets are available as GEO, GSE212470 that includes the ChIP-seq as GSE212468 and the RNA-seq as GSE212469. Publicly available datasets Repli-seq, OK-seq, and RNA-seq implemented in this study are available, respectively, at 4DN Network, experiment set 4DNESUNOW1OZ, and GEO GSE114017 and GSE146121.

Submitted 16 March 2022
Accepted 26 October 2022
Published 9 December 2022
10.1126/sciadv.abq0648

ScienceAdvances

NEDDylated Cullin 3 mediates the adaptive response to topoisomerase 1 inhibitors

Alice Meroni, Jan Grosser, Sumedha Agashe, Natasha Ramakrishnan, Jessica Jackson, Priyanka Verma, Laura Baranello, and Alessandro Vindigni

Sci. Adv., **8** (49), eabq0648.
DOI: 10.1126/sciadv.abq0648

Science Advances (ISSN) is published by the American Association for the Advancement of Science. 1200 New York Avenue NW, Washington, DC 20005. The title *Science Advances* is a registered trademark of AAAS.